

Correlation between sea-level rise and aspects of future tropical cyclone activity in CMIP6 models

Joseph W. Lockwood¹, Michael Oppenheimer^{1,2,3}, Ning Lin⁴, Robert E. Kopp^{5,6}, Gabriel A. Vecchi^{1,3,7} and Avantika Gori⁴

¹Department of Geoscience, Princeton University, NJ 08544, USA

²Princeton School of Public and International Affairs, Princeton University, Princeton, NJ 08544, USA

³High Meadows Environmental Institute, Princeton, NJ, USA

⁴Civil and Environmental Engineering, Princeton University, Princeton, NJ 08544, USA

⁵Institute of Earth, Ocean, and Atmospheric Sciences, Rutgers University, 71 Dudley Road, Suite 205,

New Brunswick, NJ 08901, USA

⁶Department of Earth and Planetary Sciences, Rutgers University, Piscataway, NJ, USA

⁷Atmospheric and Oceanic Sciences Program, Princeton University, Princeton, NJ, USA

Key Points:

- Relative sea-level rise at many locations is strongly correlated with two large-scale factors known to modulate tropical cyclone activity
- Joint increases in sea level and tropical cyclone activity with global mean temperature substantially compound flood hazard at New York City
- Flood hazard assessments that neglect the joint influence of these factors may not accurately represent future flood hazard

Corresponding author: Joseph W. Lockwood, j1115@princeton.edu

Abstract

Future coastal flood hazard at many locations will be impacted by both tropical cyclone (TC) change and relative sea-level rise (SLR). Despite sea level and TC activity being influenced by common thermodynamic and dynamic climate variables, their future changes are generally considered independently. Here, we investigate correlations between SLR and TC change derived from simulations of 26 Coupled Model Intercomparison Project Phase 6 (CMIP6) models. We first explore correlations between SLR and TC activity by inference from two large-scale factors known to modulate TC activity: potential intensity (PI) and vertical wind shear. Under the high emissions SSP5-8.5, SLR is strongly correlated with PI change (positively) and vertical wind shear change (negatively) over much of the western North Atlantic and North West Pacific. To explore the impact of the joint changes on flood hazard, we then conduct climatology–hydrodynamic modeling with New York City (NYC) as an example. Coastal flood hazard at NYC correlates strongly with global mean surface air temperature (GSAT), due to joint increases in both sea level and TC storm surges, the later driven by stronger and more slowly moving TCs. If positive correlations between SLR and TC changes are ignored in estimating flood hazard, the average projected change to the historical 100 year storm tide event is underestimated by 0.09 m (7 %) and the range across CMIP6 models is underestimated by 0.17 m (11 %). Our results suggest that flood hazard assessments that neglect the joint influence of these factors and that do not reflect the full distribution of GSAT changes will not accurately represent future flood hazard.

Plain Language Summary

Future coastal flood hazard at many locations will be influenced by sea level rise (SLR) and tropical cyclone (TC) activity. Due to their common dependence on the wider climate system, TC activity and SLR may increase in a joint manner with progressive warming, potentially acting to compound local flood hazards. To explore joint variability, we first analyze correlations between SLR and future TC activity by inference from two large-scale climate factors known to modulate TC activity. Our results indicate that flood hazard in the western North Atlantic and North West Pacific will increase with progressive warming, due to concurrent changes in relative SLR and TC activity. Using a set of realistic synthetic TC events and a storm tide model, we find that joint increases in SLR and TC activity substantially compound flood hazard at New York City, with TC surge changes driven by progressively slower and stronger TCs. Our results suggest that flood hazard assessments that neglect the joint influence of these factors and that do not reflect the full distribution of global mean surface temperature (that modulates joint changes in TC and SLR) will not accurately capture future flood hazard.

1 Introduction

Coastal flooding in the context of future tropical cyclone (TC) variability, sea-level rise (SLR) and shoreline change is one of the most important issues facing coastal populations (Woodruff et al., 2013). Climate change is increasing the threat posed by TCs to coastal regions (Reed et al., 2015; Wang & Toumi, 2021; Camargo & Wing, 2021; Knutson et al., 2020), with future flood events driven by TC storm surges expected to intensify into the future as a result of accelerated SLR (Lin et al., 2012; Woodruff et al., 2013; Bilskie et al., 2014, 2016; Reed et al., 2015; Garner et al., 2017; Vousdoukas et al., 2018; Marsooli et al., 2019; Idier et al., 2019; Liu et al., 2019; Kirezci et al., 2020; Marsooli & Lin, 2020; De Dominicis et al., 2020). At many locations, future flood hazard may also be compounded by changes in TC climatology and associated storm surges (Lin et al., 2012; Reed et al., 2015; Little et al., 2015; Lin et al., 2016; Buchanan et al., 2016; Marsooli et al., 2019; Marsooli & Lin, 2020), with SLR elevating the baseline on which these events occur. The potential compound effect of sea level change and TC activity is best

70 exemplified by supertyphoon Haiyan (2013). Observed increases in regional sea surface
71 temperatures (SST) and ocean heat content since 1993, likely contributed to both the
72 typhoon's extreme wind speeds and regional SLR. This regional SLR meant that Haiyan's
73 extreme storm surge was on a baseline sea level some 30 cm above levels in 1993 (Trenberth
74 et al., 2015).

75 Most recent flood hazard assessments generally assume that SLR and TCs are in-
76 dependent, conditional on the emissions pathway (Lin et al., 2012; Garner et al., 2017;
77 Idier et al., 2019; Marsooli et al., 2019; Marsooli & Lin, 2020). Assessments that explore
78 projected changes in TCs generally either combine storm surges with a limited number
79 of SLR scenarios (Lin et al., 2012; Bilskie et al., 2014, 2016; Idier et al., 2019; Liu et al.,
80 2019) or with probabilistic SLR projections that are derived in part from a subset of AOGCMs
81 (Lin et al., 2016; Garner et al., 2017; Vousdoukas et al., 2018; Marsooli et al., 2019; Mar-
82 sooli & Lin, 2020). On the other hand, assessments that evaluate changes in flood haz-
83 ard due to SLR usually assume that the statistical nature of TC storm surges will re-
84 main unchanged (Hunter, 2011; Tebaldi et al., 2012; Buchanan et al., 2016; Rasmussen
85 et al., 2018; Kopp et al., 2014, 2017; Frederikse et al., 2020; Kirezci et al., 2020). By ne-
86 glecting concurrent changes (Hunter, 2011; Tebaldi et al., 2012; Buchanan et al., 2016;
87 Rasmussen et al., 2018; Kopp et al., 2014, 2017; Frederikse et al., 2020; Kirezci et al.,
88 2020) or by assuming independence conditional on the emissions scenario (Lin et al., 2012;
89 Garner et al., 2017; Idier et al., 2019; Marsooli et al., 2019; Marsooli & Lin, 2020), as-
90 sements may fail to fully represent compounding of future flood hazard.

91 Recent research shows that dependence structures between climate variables often
92 strongly affects the occurrence frequency and intensity of multivariate extremes (Little
93 et al., 2015; Wahl et al., 2015; Zscheischler & Seneviratne, 2017; Zscheischler et al., 2018).
94 At present, there is limited analysis of the dependence between SLR and TC activity,
95 and its implications for coastal flood hazard. Little et al. (2015) project changes in surge
96 hazard focusing on sterodynamic SLR, composed of ocean thermal expansion and regional
97 ocean steric and dynamic effects (Gregory et al., 2019), and power dissipation index (PDI)
98 changes at 5 sites along the US East Coast — the latter derived from a 15-member en-
99 semble of climate models following a statistical modeling approach (Villarini & Vecchi,
100 2013). Sterodynamic SLR and PDI projections along the US East Coast are found to
101 be correlated, with joint increases compounding projected flood hazard. However, the
102 projected increases in Atlantic PDI have considerable uncertainty, as several other TC
103 modeling studies using dynamical, rather than statistical, downscaling approaches project
104 little change or decreases in PDI (Yamada et al., 2010; Knutson et al., 2015) .

105 Joint variability between SLR and TCs will be driven in part by atmospheric warm-
106 ing, which will increase SLR through ocean heat uptake and thermal expansion and by
107 melting land ice (Church et al., 2013; Oppenheimer et al., 2019) as well as the theoret-
108 ical maximum wind speed (the potential intensity; PI) of TCs in some regions (Vecchi
109 & Soden, 2007a, 2007c; Emanuel, 2013; Sobel et al., 2016). Basin-specific changes in ver-
110 tical wind shear, another important large-scale variable modulating TC activity, are pro-
111 jected with warming, with increases across the tropical North Atlantic and decreases across
112 the northern tropical Pacific and western North Atlantic (Vecchi & Soden, 2007a, 2007c;
113 Camargo, 2013; Vecchi et al., 2019), which would suggest less conducive conditions for
114 TC activity in the former and more conducive conditions in the latter.

115 Considerable uncertainty remains in the projection of future TCs, particularly re-
116 garding changes in frequency, translation speed and average latitude at which TCs reach
117 their lifetime-maximum intensity (Knutson et al., 2020), and their dependence on the
118 large-scale climate. Low-resolution AOGCMs, which are often used to investigate TCs,
119 generally cannot resolve category 3–5 TCs or poorly simulate the frequency and spatial
120 distribution of category 3–5 TCs compared to observations (Vecchi et al., 2019; Knut-
121 son et al., 2020; Yin et al., 2020). These low resolution AOGCMs generally project de-
122 creases in global TC frequency under climate change (Knutson et al., 2020). In contrast,

123 some studies project no change (Camargo, 2013; Vecchi et al., 2019) or increases in global
124 TC frequency (Emanuel, 2013; Bhatia et al., 2018; Vecchi et al., 2019; Emanuel, 2021).
125 As reviewed by Knutson et al. (2020), there is moderately strong consensus on a model-
126 projected increase in high intensity TCs, in TCs rainfall and in an increase in storm-surge
127 flooding due to SLR, assuming all other factors are unchanged.

128 Superimposed on the global SLR, that is driven by ocean thermal expansion and
129 by melting land ice loss, relative sea levels may change owing to vertical land movement
130 (VLM) and dynamic sea level changes. The steredynamic component of relative SLR
131 is derived from AOGCMs that do not simulate SLR contributions from melting land ice
132 and local non-climatic SLR associated with VLM and glacial isostatic adjustment (GIA)
133 (Kopp et al., 2014, 2015; Griffies et al., 2016; Gregory et al., 2019). Estimates of land
134 ice contributions to SLR are instead derived from physical models of varying degree of
135 complexity (Levermann et al., 2020; Oppenheimer et al., 2019) or from results of struc-
136 tured expert elicitation (Bamber et al., 2019). In probabilistic analyses, variance in global
137 mean sea level rise (GMSLR) and local SLR at many locations in the early 21st century
138 relates predominately to steredynamic SLR, due to large AOGCM spread in projected
139 changes (Kopp et al., 2014, 2017). In the global average and at many locations, the Antarc-
140 tic ice-sheet is the dominant source of variance in late 21st century SLR projections (Kopp
141 et al., 2014, 2017).

142 Although there is strong confidence in accelerated SLR intensifying TC storm surge
143 into the future, only a limited number of studies have assessed the role of their joint changes
144 to future multivariate extreme events, in part due to the large uncertainties discussed
145 above. The questions to be answered in this paper are as follows: (i) Are relative SLR
146 and aspects of TC activity (PI and vertical wind shear) correlated within the wider cli-
147 mate system, and what are the time scales and emissions scenarios over which these cor-
148 relations apply? (ii) Do the broad-scale joint changes translate into meaningful differ-
149 ences in flood hazards at a local scale? To answer these questions, we first investigate
150 correlations between relative SLR and TC activity derived from simulations of 26 CMIP6
151 models, across a range of emissions scenarios. We next conduct climatology-hydrodynamic
152 modeling for eight CMIP6 models under SSP5-8.5 to quantify the impact of joint changes
153 to future coastal flood events, as an example, for New York City (NYC).

154 2 Methods

155 CMIP6 models comprise a range of AOGCMs and Earth System Models (ESMs),
156 differing from each other in terms of model structure, including vertical coordinate, grid
157 resolution and sub-grid parameterizations (Eyring et al., 2016). We limit our analysis
158 to models that have the variables necessary to compute PI, relative SLR and vertical wind
159 shear. We use only a single run ('r1i1p1') for each CMIP6 model. Change is calculated
160 as the difference between years 1994-2014 of the historical simulation and years 2080-
161 2100 of the high emissions SSP5-8.5, unless otherwise stated. Our primary focus on SSP5-
162 8.5, which has unrealistically high anthropogenic carbon dioxide emissions (Hausfather
163 & Peters, 2020), allows us to maximize the signal of interest. To explore the time pe-
164 riods and scenarios over which these correlations apply, we also calculate relative SLR
165 and PI over years 2014-2100 of the SSP1-2.6, SSP2-4.5 and SSP5-8.5 scenarios for 11 CMIP6
166 models. These 11 models span the full range of GSAT changes projected by the 26 CMIP6
167 models used in this study (Fig. S1 a). The goal of our SLR projections is to produce SLR
168 projections consistent with the GSAT of each model. We note that the methods used
169 to project SLR have considerable uncertainties; however, we choose to focus
170 on the mean projection for each model.

2.1 SLR projections

2.1.1 Sterodynamic sea-level change

Sterodynamic SLR ($\Delta Z(r)$) is calculated as the linear addition of changes in ocean dynamic sea level ($\Delta \zeta$) and global thermosteric sea level (Δh_θ) following Gregory et al. (2019). It can be diagnosed from CMIP6 model variables as the sum of the changes in zos ($\Delta \zeta(r)$) and zostoga (Δh_θ):

$$\Delta Z(r) = \Delta \zeta(r) + \Delta h_\theta \quad (1)$$

Dynamic sea level fluctuations, due to regional ocean steric and dynamic effects, are calculated as the local height of the sea surface above the geoid with zero global mean (Gregory et al., 2019), so that it measures sea-level pattern fluctuations around the ocean geoid defined via a resting ocean state at $z = 0$, as defined in Griffies and Greatbatch (2012) and Griffies et al. (2014). As some models used in this study do not have zostoga output, we calculate h_θ using potential temperature (Text S1.1).

2.1.2 Antarctic Ice Sheet

To derive future Antarctic Ice Sheet (AIS) dynamical SLR estimates we utilize the impulse response functions by Levermann et al. (2020). Specifically, Levermann et al. (2020) related subsurface ocean warming in Antarctica to projected GSAT change based on an ensemble of CMIP5 models. Estimated basal melt sensitivities from observations were then used to translate subsurface ocean warming into basal ice-shelf loss projections using 16 ice-sheet models that form part of the Linear Antarctic Response Model Intercomparison Project (LARMIP-2).

Following Levermann et al. (2020), we estimate AIS contributions using an ice shelf melt rate of 8 m year^{-1} for each CMIP6 model (Fig. S2). We note that these estimates have considerable uncertainties related to basal ice shelf melt rates, ice sheet models and scaling factors (Fig. S2). We convert global barystatic contributions to regional values using the output from a Gravitation, Rotation, and Deformation (GRD) model (Tamisiea & Mitrovica, 2011), assuming uniform mass loss for each individual region. The regional imprint of mass loss from the Amundsen sector and the Antarctic peninsula are based on uniform mass loss from West Antarctica. The contribution from East Antarctica and the Weddell and Ross sector is distributed based on the assumption of uniform mass loss from East Antarctica.

In assuming linear response theory, this method is able to capture complex temporal responses of the ice sheets, but neglects any self-dampening or self-amplifying processes. Neglecting self-amplifying processes is particularly relevant in situations in which an instability is dominating the ice loss such as during Marine Ice Sheet Instability (MISI) and Marine Ice Cliff Instability (MICI), although there remains major uncertainty in the possibility of rapid and/or irreversible ice losses via these mechanisms (Fox-Kemper et al., 2021).

The observed evolution of the Amundsen Sea Embayment (ASE) glaciers is compatible with, but not unequivocally indicating an ongoing MISI (Rignot et al., 2014; Joughin et al., 2014; Fox-Kemper et al., 2021). There remains significant discrepancies in projections of MISI due to poor understanding of mechanisms and lack of observational data to constrain ice-sheet models, and it is not expected that widespread loss from the large ice shelves buttressing the bulk of West Antarctic Ice Sheet will occur before the end of the 21st century (Fox-Kemper et al., 2021). The International Panel on Climate Change (IPCC) Sixth Assessment Report (AR6) (Fox-Kemper et al., 2021) assigned limited agreement (with an assessed likelihood of 0-33%) between studies regarding the exact MICI mechanism and limited evidence (likelihood of 0-33%) of its occurrence in the present or the past, meaning that MICI considered to be characterized by deep uncertainty, and

its potential to affect future sea level rise is currently highly uncertain (Oppenheimer et al., 2019; Edwards et al., 2021; Fox-Kemper et al., 2021). These strong caveats that are associated with the approach utilized here, that neglects MISI and MICI, may lead to an underestimation of future dynamical ice loss. Nonetheless, this method provides model specific estimates of Antarctica’s future dynamical contribution to SLR.

Following the International Panel on Climate Change (IPCC) Sixth Assessment Report (AR6) (Fox-Kemper et al., 2021), we augment LARMIP-2 estimates with surface mass balance (SMB) estimates. SMB estimates derived directly from GCMs often involve several compromises related to their coarse resolution and their low sophistication to represent important physical processes of polar regions. In addition, SMB consists of multiple components, all of which depend on complex interactions between the atmosphere and the snow/ice surface, large-scale atmospheric circulation and ocean conditions, and ice sheet topography (Kittel et al., 2021). As a result of the complex nature of SMB estimation, and the fact that many GCMs tend to overestimate annual precipitation values over ice-sheets, likely due to poor representation of coastal topography (Genthon et al., 2009), this study parameterizes SMB to estimate SLR contributions for the AIS. Parameterizations are derived from relationships between SMB changes and atmospheric temperature using high resolution regional climate models. For each model, we average estimates derived from the parameterizations of Gregory and Huybrechts (2006) and Kittel et al. (2021) to estimate AIS SMB changes (Text S1.2).

2.1.3 Greenland Ice Sheet

Simulating the changes in continental-scale mass balance (MB) in Greenland Ice Sheet (GIS) models remains challenging due to the small scale of key physics, such as fjord circulation and plume dynamics, and poor understanding of critical processes, such as calving and submarine melting. Fürst et al. (2015) used ten different CMIP5 AOGCMs simulations to provide MB and ocean forcing for their GIS model, accounting for influences of warming subsurface ocean temperatures and basal lubrication on ice dynamics. We model GIS loss using estimates from Fürst et al. (2015), where GIS MB can be estimated as a cubic function of near-surface temperature anomaly over the GIS (Fig. S3):

$$\Delta MB_{GIS} = 0.030T_{GrIS}^2 - 0.81T_{GrIS} + 2.2 \quad (2)$$

where TAS_{GrIS} is the average anomaly in near-surface temperature over the GIS.

In Greenland, faster-than-projected changes in mass loss might occur into the future (Aschwanden et al., 2019; Khan et al., 2020) due to cloud processes in polar areas (Hofer et al., 2019) and feedbacks between surface melt and the increasing albedo from meltwater, detritus and pigmented algae (Cook et al., 2020). Warming-induced dynamical changes in atmospheric circulation could enhance summer blocking and produce more frequent extreme melt events over Greenland that may also enhance future mass loss (Delhasse et al., 2018).

2.1.4 Glaciers and Ice Caps

Over the past century, glaciers and ice caps (GIC) have added more mass to the ocean than the GIS and AIS combined. However, the total remaining mass of glaciers is small by comparison, equivalent to only 0.32 m mean SLR if only the fraction of ice above sea level is considered (Farinotti et al., 2019). We model GIC following Perrette et al. (2013), where the rate of glacier’s ice loss is proportional to a change in GSAT:

$$\frac{dV}{dt} = b_o(T - T_o)\left(1 - \frac{V_{gl}}{V_o}\right)^n \quad (3)$$

where b_o is the global SMB sensitivity, V_{gl} and V_o are the projected and present global glacier volumes (in sea level equivalent) respectively, and n is the scaling coefficient be-

265 tween global glacier area and volume, approximately equal to 1.65 (Perrette et al., 2013).
 266 T is the GSAT change as compared to the 1994-2014 historical temperature (T_o). The
 267 spatial pattern used here assumes a fixed distribution of the ratios of glacier mass loss
 268 between the glacier regions based on the projected distribution in 2100 under Represent-
 269 ative Concentration Pathway 8.5 (RCP8.5) (Church et al., 2013). Previous analysis showed
 270 that this pattern does not vary much over the 21st century and the mass loss is closely
 271 related to the initial glacier mass for a given region. Recent studies have shown that the
 272 mass loss distribution to be model and scenario dependent (Hock et al., 2019; Marzeion
 273 et al., 2020).

274 **2.1.5 Non-climatic SLR**

275 Changes in land water storage, through groundwater depletion and reservoir im-
 276 poundment, may have influenced twentieth-century sea-level change but are expected
 277 to be relatively minor contributors (Church et al., 2013). We adopt the methods of Kopp
 278 et al. (2014) to model land water storage change. Ongoing GIA also leaves its imprint
 279 in the spatial pattern of sea-level change, associated with the adjustment of Earth's litho-
 280 sphere and viscous mantle material to past changes in ice loading since the last glacia-
 281 tion (e.g., Tamisiea and Mitrovica (2011)). This adjustment process gives rise to areas
 282 of upward and downward VLM, and the associated mass redistribution also influences
 283 Earth's rotation and gravity field with additional impacts on local mean sea level. We
 284 use global GIA estimates based on the ICE-6G_C model of Peltier et al. (2015), which
 285 uses a wide range of observational constraints, including data from Global Positioning
 286 System receivers and time-dependent gravity observations from both surface measure-
 287 ments and the satellite-based Gravity Recovery and Climate Experiment (Argus et al.,
 288 2014; Peltier et al., 2015). This data set was sourced from [https://www.atmosp.physics](https://www.atmosp.physics.utoronto.ca/~peltier/data.php)
 289 [.utoronto.ca/~peltier/data.php](https://www.atmosp.physics.utoronto.ca/~peltier/data.php). We note that this term is not relevant to our anal-
 290 ysis, since it is independent of climate forcing and constant across models, but does af-
 291 fect projections of flood risk in NYC.

292 **2.2 Large-scale factors affecting TC activity**

293 As low-resolution climate models are better able to simulate the large-scale envi-
 294 ronment, rather than individual TCs, many studies have chosen to analyze large-scale
 295 variables known to be associated with TC activity, instead of modeling TCs directly (Camargo,
 296 2013; Tang & Camargo, 2014; Vecchi et al., 2019; Emanuel, 2021). Following Bister and
 297 Emanuel (1998), we calculate PI as a function of both the SST and the vertical profiles
 298 of temperature and humidity in the atmosphere. Although PI is a prediction only of the
 299 maximum intensity that a TC can achieve in a given environment, it is expected to pro-
 300 vide a useful guide to the statistical distribution of actual intensities achieved by real TCs
 301 (Sobel et al., 2016). Most TCs do not achieve their PI because of a variety of negative
 302 influences (e.g., vertical wind shear and ocean cooling effects).

303 We explore vertical wind shear, with weak vertical wind shear being favorable for
 304 hurricane convective organization and intensification (Merrill, 1988; Rios-Berrios & Torn,
 305 2017). Vertical wind shear is calculated as the magnitude of the vector difference of wind
 306 velocity at 850 hPa and 200 hPa, computed from monthly-mean output. Increases in PI
 307 and decreases in vertical wind shear suggest an environment more conducive to future
 308 TC activity (Bister & Emanuel, 1998; Emanuel & Nolan, 2004; Emanuel, 2013).

309 **2.3 Hydrodynamic-climatological modeling**

310 Storm tide (combination of astronomical tide and storm surge) projections are based
 311 on simulations of Gori et al. (under review), using the 2D depth-integrated version of
 312 the hydrodynamic model ADvanced CIRCulation (ADCIRC) (Luettich et al., 1992; Wes-
 313 terink et al., 1994). We model storm tides for each of the eight CMIP6 models (herein

ADCIRC-CMIP6 models) that overlap with the study of Gori et al. (under review) (see Fig. 4 for the models) for the time periods and simulations employed in this study. TCs are modeled using the statistical-deterministic hurricane model developed by Emanuel et al. (2008) and Emanuel (2021). The ADCIRC mesh has a resolution of between 1 km nearshore and 100 km in the deep ocean (Marsooli et al., 2019; Lin et al., 2019; Gori et al., under review). Additionally, we focus only on synthetic TCs that pass within 200 km of NYC. Storm surges induced by TCs result in devastating flood events in NYC, as best exemplified by historical TCs such as Hurricane Donna in 1960 and Sandy in 2012. Following Lin et al. (2012), we assume the cyclone-threatened area for NYC to be within a 200-km radius from the Battery (74°W, 40.9°N; chosen as the representative location for NYC).

Previous work by Marsooli and Lin (2018) demonstrated that the impact of wave setup near NYC is relatively small; thus we do not include waves in our simulations. Statistical analysis is performed on the modeled peak storm tides to produce return period curves for each model. Flood return periods presented here are bias-corrected by comparing NCEP-based storm tide projections for the historical period with model-based projections on TC intensity for the same historical period and assuming the same bias in the future period. Assuming that the storms arrive as a stationary Poisson process under a given climate, the return period of TC-induced storm tide η_{TC} exceeding a given level h is (Marsooli et al., 2019):

$$\eta_{TC} = \frac{1}{Fr(1 - P\{\eta_{TC} \leq h\})} \quad (4)$$

where $P\{\eta_{TC} \leq h\}$ is the cumulative probability distribution (CDF) of peak storm tide and Fr is the TC annual frequency. Here, we model the tail of the storm tide CDF using the Peaks-Over-Threshold method with a Generalized Pareto Distribution and maximum likelihood estimation (Coles, 2001). Non-parametric density estimations are used to model the rest of the distribution. We determine the tail threshold value by trial and error so that the smallest error in the distribution fitted to the tail is obtained.

3 Results

3.1 Future SLR and factors affecting TC activity

We present the CMIP6 ensemble mean relative SLR as a difference between years 1994–2014 of the historical simulation and years 2080–2100 of the SSP5-8.5 simulation (Fig. 1 a). GMSLR is 0.68 m, slightly larger than the AR6 estimate of 0.64 m (17th - 83rd percentile ranges of 0.52 - 0.83 m) in 2090 (Fox-Kemper et al., 2021), with projections across the ensemble positively correlated with GSAT change ($\rho = 0.82$; Fig. S4 a). Our ensemble estimates of GIC (0.16 m), thermal expansion (0.26 m) and GIS (0.1 m) (Fig. S5) are consistent with respectively values reported in AR6 of 0.15 m, 0.25 m and 0.1 m in 2090 (Fox-Kemper et al., 2021).

GMSLR projected here is higher than CMIP6 estimates presented in AR6 due predominantly to the different methods used to project AIS contributions to GMSLR, with our results being 0.043 m higher (Fig. S5). In AR6, for processes in whose projections have at least medium confidence (with an assessed likelihood of 66-100%), projections for the AIS up to 2100 are estimated from a p-box that combines simulations from emulations of the Ice Sheet Model Intercomparison Project for CMIP6 (ISMIP6) (Edwards et al., 2021) and LARMIP-2 simulations (Levermann et al., 2020) augmented by AR5 surface mass balance model. ISMIP6 and LARMIP-2 projections in AR6 were estimated using CMIP6 GSAT distributions from a two-layer energy budget emulator (Fox-Kemper et al., 2021). Here, we utilize only the LARMIP-2 simulations (Levermann et al., 2020) augmented with two similar surface mass balance models to AR5. As noted in AR6, LARMIP-

2 median projections are higher than those of the ISMIP6 emulator, although AR6 could not distinguish which of ISMIP6 and LARMIP-2 is more realistic due to limitations in historical simulations and understanding of basal melting (Fox-Kemper et al., 2021).

21st century SLR scales with regional temperature change at approximately 0.15 and 0.14 m per degree in the western western North Atlantic and North West Pacific, respectively (Fig. 1 d,g; regions defined in Fig. 1 a). GMSLR also scales with GSAT change increase at an average rate of 0.11 m per degree across the ensemble. Relative SLR in the western North Atlantic and North West Pacific exceeds the global mean rate in part due to regionally high stericodynamic changes and as a consequence of the higher than global mean barostatic SLR associated with the spatial GRD fingerprints (Fig. S6 a-d). We note that future AIS contributions to SLR derived here will likely not scale with GSAT, as incorporating MISI and MICI in our AIS projections may further augment differences between models (Vega-Westhoff et al., 2020).

Whilst the CMIP6 ensemble mean June–November PI increases over most of the northern hemisphere tropics, there is a large region in the northern tropical Atlantic where the ensemble-mean PI decreases (Fig. 1 b). Projections of PI in CMIP3 (Vecchi & Soden, 2007a, 2007c) and CMIP5 models (Camargo, 2013; Sobel et al., 2016) have very similar patterns in the Northern Hemisphere to that shown here. In agreement with Vecchi and Soden (2007a, 2007c), we find that PI changes around the globe closely follow the structure of SST changes – with regions that warm more (less) than the tropical mean (relative SST; averaged over 35°S - 35°N) showing a PI increase (decrease) (Fig. 1 b). CMIP6 models project an average PI increase of 4.5% and 5.2% per degree regional temperature warming in the western North Atlantic and North West Pacific, respectively (Fig. 1 e,h). Globally averaged PI increases at a rate of 2.3 % per degree GSAT warming, consistent with an increase of 5% (likely range 1 to 10%) per two degrees warming as estimated in Knutson et al. (2020).

Using a subset of CMIP6 models, Hermans et al. (2021) found that global mean sea level (GMSL) scales with integrated GSAT, with most of the contributors to GMSL being more closely tied to time-integrated GSAT than instantaneous GSAT, meaning that sea level projections can only be interpreted if the warming levels are linked to a specific time-frame (Fox-Kemper et al., 2021). In contrast to GMSL, using a subset of CMIP6 models, we find that globally averaged PI appears to scale with instantaneous GSAT in a time- and scenario-independent manner (Fig. S7). Thus, the rates of increase in PI per degree GSAT change found here will likely be constant regardless of time or emissions scenario.

Basin-specific changes in vertical wind shear are projected, with increases across the tropical Atlantic and decreases across the northern tropical Pacific and western North Atlantic (Fig. 1 c). The CMIP6 model mean pattern is similar to that obtained in CMIP3 (Vecchi & Soden, 2007c) and CMIP5 (Camargo, 2013; Ting et al., 2019) models for the Northern Hemisphere TC season. These changes in vertical shear are associated to the projected decrease in the Pacific Walker circulation (Vecchi & Soden, 2007c), while the near-equatorial vertical shear weakening reflects a reduction of zonal overturning (Vecchi & Soden, 2007b, 2007c).

Projected changes to vertical wind shear over the ocean in the western North Atlantic and North West Pacific are -2.2 % and -2.7 % per degree regional temperature warming, respectively (Fig. 1 f,i). Reducing vertical wind shear in these regions is consistent with the expected expansion of the Hadley circulation (Lu et al., 2007; Kang & Lu, 2012), and the related northward shift of the midlatitude jet stream (Ting et al., 2019). To determine the change in vertical wind shear due to contributions from the upper and lower levels, Figure 2 shows the wind vector differences between the two periods. The intensification and northward shift of the midlatitude jet is clearly seen at both the upper and lower levels in the Atlantic and the Pacific, being stronger and more defined in models

413 that project higher GSAT warming (Fig. 2 c,f). In agreement with a similar analysis of
 414 CMIP5 models (Ting et al., 2019), there is some indication of a southward flow at the
 415 lower level and northward flow at the upper level, implying an enhanced and northward
 416 extended Hadley circulation (Fig. 2 c,f).

417 Large inter-model differences exist: the CMIP6 model with the highest GSAT change
 418 (CanESM5; GSAT of 7.0°C) projects a GMSLR of 0.98 m and a 4% increase in globally
 419 averaged PI, whereas, the model with the lowest GSAT (CAMS-CSM1-0; GSAT of 2.8°C)
 420 projects a GMSLR of 0.61 m and an 8% increase in globally averaged PI (Fig. S4). Inter-
 421 model spread is strongly related to GSAT change, which is positively correlated to GM-
 422 SLR ($\rho = 0.82$) and globally averaged PI ($\rho = 0.62$; Fig. S4). Additionally, models fall
 423 roughly at the same position in the CMIP6 ensemble SLR and PI change distributions
 424 in the western North Atlantic when compared to the North West Pacific (e.g. CAMS-
 425 CSM1-0 projects the lowest average relative SLR and PI change in both regions; Fig. 1),
 426 suggesting that changes are coupled and are related by global mean changes.

427 Hence, in CMIP6 models, GMSLR and global mean PI change are closely related
 428 to GSAT change, whilst spatial patterns in PI change are tightly coupled with spatial
 429 changes in relative SST. Vertical wind shear tendencies are spatially more complex. In
 430 the western North Atlantic and North Pacific, vertical wind shear responds to changes
 431 in the mid-latitude jet, which is generally stronger in CMIP6 models that project higher
 432 GSAT change. As the climate system is strongly coupled, global and regional co-variability
 433 between SLR and TC activity, shown here to be related to GSAT change, may impose
 434 correlations between these variables. We next explore these correlations.

435 3.2 Correlation between SLR and large scale factors affecting TCs

436 The inter-model correlation is computed as the rank correlation across the CMIP6
 437 ensemble between SLR and TC activity in historical and future (SSP5-8.5) simulations
 438 (Fig. 3). There are strong positive correlations between PI change and relative SLR in
 439 most regions: models with large PI increases show higher projected relative SLR (Fig-
 440 ure 3 a). This strong SLR-PI relationship is consistent with both being broadly related
 441 to GSAT change (see Section 3.1). To explore the time periods and scenarios over which
 442 these correlations apply, we calculate intra-model correlations between relative SLR and
 443 PI change (Fig. S8). Intra-model correlations are calculated over the full 86 years of the
 444 SSP1-2.6, SSP2-4.5 and SSP5-8.5 scenarios for 11 CMIP6 models. The spatial patterns
 445 of intra-model correlations are very similar across scenarios, however, the correlation co-
 446 efficients are stronger over time and in the higher emissions scenarios (Fig. S8). The rea-
 447 son for this difference may be due to larger ratio of forced signal to internal variability
 448 for later time period and for higher emissions scenarios. SLR contributions from land
 449 ice loss are strongly correlated with PI and vertical wind shear change in the western North
 450 Atlantic and North West Pacific (Fig. 3 e-j). SLR from land ice loss follows the spatial
 451 patterns of GRD fingerprints that is constant across models, meaning that the spatial
 452 correlations between TC activity and barystatic SLR are a result of common relations
 453 to global mean changes, rather than as a result of regional co-variability.

454 Relative SLR and vertical wind shear show regionally variable inter-model corre-
 455 lations (Fig. 3 b), that largely follows the spatial pattern of the ensemble mean verti-
 456 cal wind shear change (Fig. 1 c), being strongly negative in the western North Atlantic
 457 and North West Pacific, whilst positive in the tropical Atlantic region. Additionally, we
 458 find that PI and vertical wind shear are negatively correlated in parts of the western North
 459 Atlantic and North West Pacific (Fig. S9). The projected weakening of the vertical wind
 460 shear environment in the western North Atlantic and North West Pacific may help TCs
 461 reach their PI into the future. As PI and vertical wind shear are anti-correlated over much
 462 of the western North Atlantic and North West Pacific (Fig. S9), based solely on these
 463 metrics, we may well expect a non-linear increase in TC intensity.

464 The increases in PI across the western North Atlantic and North West Pacific, cou-
 465 pled with the more favorable vertical wind shear change suggests a large scale environ-
 466 nment more conducive to TC intensification, with TCs having a better chance of achiev-
 467 ing higher PIs in these regions (Ting et al., 2019). Additional and concurrent increases
 468 in relative SLR, suggest a significant and compounding intensification of flood hazard
 469 in these regions, based solely upon these metrics. For the Gulf Coast and tropical At-
 470 lantic, the future projected increase in vertical wind shear may induce a reduction of the
 471 intensity of strong landfalling TCs, although the increase in PI there may outweigh the
 472 effect of increasing vertical wind shear.

473 We have found strong inter- and intra-model correlations between SLR and TC ac-
 474 tivity change, with GSAT change being the key physical mechanism driving co-variability
 475 (Section. 3.1). The correlations between TC activity and relative SLR, may in turn af-
 476 fect the occurrence frequency and intensity of multivariate extreme events along the coast.
 477 We next explore the extent to which joint changes impact future coastal flood events at
 478 NYC.

479 3.3 Implications for Coastal Flooding at NYC

480 3.3.1 Future changes to the storm tide

481 Synthetic TCs used in this study are generated for the NYC area using the statistical-
 482 deterministic hurricane model of Emanuel et al. (2008) and Emanuel (2021). The TC
 483 model generates synthetic TCs for a given large-scale atmospheric and oceanic environ-
 484 nment. Figure 4 presents the estimated storm surge return levels projected under the fu-
 485 ture climate, compared with those of the historical period (1994-2014), for NYC. In agree-
 486 ment with prior studies (Lin et al., 2012; Marsooli et al., 2019; Marsooli & Lin, 2020;
 487 Gori et al., under review), the storm tide level for a given return period substantially in-
 488 creases by the end of 21st century, due to relative SLR as well as TC climatology change.
 489 To quantify future flood hazard, we focus on the change in the 100-year storm tide level
 490 ($\Delta\eta_{100}$). Our projections show an increase of between 0.87 m and 2 m, with an average
 491 increase of 1.46 m (Fig. 4 j).

492 The increase in $\Delta\eta_{100}$ for each model at NYC is evidently related to each model's
 493 GSAT change and effective climate sensitivity (ECS) (Fig. 4 a-h and Table. 1). For ex-
 494 ample, changes to the $\Delta\eta_{100}$ for GFDL-ESM4 (GSAT = 3.6°C) is 0.87 m (TC only =
 495 0.19 m; SLR only = 0.68 m). For CanESM5 (GSAT = 7.0°C) the projected increase is
 496 1.7 m (TC only = 0.60 m; SLR only = 1.1 m) (Fig. 4 i). Importantly, relative SLR and
 497 TC climatology change generally both increase in a concurrent manner with GSAT change
 498 across models. A notable exception is EC-Earth3, which projects a large TC climatol-
 499 ogy increase, which can be attributed, in part, to a very large increase in TC frequency
 500 for this model (Table. 1). The difference in projected $\Delta\eta_{100}$ between the models with
 501 the lowest (GFDL-ESM4) and highest (CanESM5) projected GSAT change, incorporat-
 502 ing each models own relative SLR and TC change, is 0.83 m at NYC by 2080-2100 (Fig.
 503 4 i).

504 In our simulations, changes to storm frequency for NYC are large in the future (Ta-
 505 ble. 1). As TC frequency is a major uncertainty in the projections of TCs (Knutson et
 506 al., 2020), we repeat our analyses assuming that there is no change in annual frequency
 507 (Fig. 4 j and Fig. S10). By neglecting changes in TC frequency, projected TC storm surge
 508 changes are substantially reduced at NYC, with models that projected low GSAT change
 509 now projecting little change to TC storm tides (Fig. 4 k). We still, however, find evi-
 510 dence of concurrent increases in TC climatology with relative SLR and GSAT change
 511 at NYC. For example, CanESM5 projects an increase of $\Delta\eta_{100}$ of 1.27 m (TC only =
 512 0.17 m; SLR only = 1.1 m), whilst GFDL-ESM4 projects an increase to the $\Delta\eta_{100}$ of 0.7
 513 m (TC only = 0.019 m; SLR only = 0.68 m). Changing storm tide levels driven by TC

514 climatology change suggest that TC intensity, track, size and translation speed could change
515 by the end of 21st century. We next explore these metrics.

516 **3.3.2 Changing TC characteristics**

517 We find that the TC track exhibits little variability along the US East Coast into
518 the future (Fig. 5 a and Fig. S11 a-h). In contrast to our results, the downscaling model
519 of Garner et al. (2017) projected using three CMIP5 models that climate change impacts
520 on TC, apart from SLR, has little net influence on storm surge hazard in the region by
521 2100, as TC tracks shifted away from landfall in the region under climate change, which
522 offset the effect of storm strengthening. We note that MIROC6 exhibits a similar track
523 shift to that found in Garner et al. (2017) (Fig. S11 b) and little change in very low prob-
524 ability surge heights (Fig. 4 b).

525 The movement of TCs tracks, is predominately determined by the steering winds,
526 with modifications due to the beta effect (Chan, 2005), the former being strongly related
527 to the position and strength of the subtropical highs. In general agreement with CMIP3
528 (26 models in Li et al. (2012)) and CMIP5 models (13 models in Li et al. (2013) and 20
529 models in Camargo (2013)), we find a significant intensification of the North Atlantic
530 subtropical high (Fig. 5 b-c and Fig. S11 i-p), which has been related to an increase in
531 thermal contrast between the land and ocean (Li et al., 2012). CMIP6 models mean sea-
532 level pressure (SLP) differences indicate that future SLP is significantly higher (100 Pa)
533 over the North Atlantic Ocean and lower over the United States (Fig. 5 b-c and Fig. S11
534 i-p). Additionally, mean SLP differences of all 26 CMIP6 models suggest a more west-
535 ward pattern in the North Atlantic subtropical high compared to the ADCIRC-CMIP6
536 subset (Fig. 5 c). These changes in SLP support our finding that the tracks of TCs that
537 affect NYC will not be substantially shifted away from the coast into the future.

538 The flooding potential, and to some extent the wind damage, caused by TCs can
539 be strongly affected by their translation speed. Slower TCs allow winds to blow onshore
540 for longer periods of time, resulting in possibly larger and longer coastal flooding. Our
541 analysis of TC translation speed and intensity (maximum wind speed) also reveals an
542 increase in the number of slow-moving and stronger TCs along the US East Coast (Fig.
543 6 a-b and Fig. S12-13). At NYC, models that project higher GSAT change and relative
544 SLR, project considerably slower and more intense TCs than low GSAT change mod-
545 els (Table. 1). For example, synthetic TCs derived from CanESM5 suggest changes to
546 TC intensity and translation speed of 25% and -29% respectively, whilst GFDL-ESM4
547 projects changes of 7.6% and -5.9% (Table. 1).

548 We utilize the complete wind profile of Chavas et al. (2015) to estimate the radius
549 of maximum wind speed, where projected decreases in radius of maximum wind speed
550 are consistent with increases in maximum wind speed, assuming constant TC outer sizes
551 (Chavas et al., 2016; Knutson et al., 2015). As TC intensity is projected to increase, we
552 find that the radius of maximum wind speed also decreases along the US East Coast (Fig.
553 6 c and Fig. S14). With progressive warming, TCs may therefore have smaller radius
554 of maximum wind speed, which may act to counteract storm surge increases driven by
555 stronger and slower moving TCs.

556 We also explore inter-model correlations between relative SLR and projected changes
557 in TC characteristics (Fig. 6 d-f). Relative SLR is positively correlated with TC inten-
558 sity, and negatively correlated with translation speed and radius of maximum wind speed
559 in the NYC region. Based on these correlations, we can deduce that compounding of in-
560 creased flood hazard at NYC with relative SLR and GSAT warming will likely be driven
561 by stronger and slowing moving TCs and possibly their increased frequency, that may
562 be counteracted in part by TCs with smaller radius of maximum wind speed.

563

3.3.3 Implications for coastal flood modeling

564

565

566

567

568

569

570

571

572

573

574

575

We have found that relative sea levels and TC storm surges both increase strongly with GSAT warming at NYC. In this section, we evaluate (1) the extent to which studies misrepresent future flood hazard by assuming independence conditional on the emissions scenario and (2) the impact of model selection bias on projected changes to flood hazard. To explore (1), we calculate the flood hazard through the convolution of the distributions of storm tide and SLR, assuming they are statistically independent (Marsooli et al., 2019). We compare the ADCRIC-CMIP6 projection that includes correlated changes (dark blue bars on Fig. 4 i-j) with the ADCRIC-CMIP6 projection obtained through convolution (light blue bars on Fig. 4 i-j). We find that by neglecting positive correlation between SLR and TC surge change, the projection of $\Delta\eta_{100}$ is under-estimated by 0.08 m (6%) and 0.05 m (5%) assuming frequency changes and no frequency change, respectively.

576

577

578

579

580

581

582

583

584

585

586

587

588

589

590

591

Inter-model differences in relative SLR and TC change indicate that selection bias may substantially alter the projected change in flood hazard at NYC. For example, the ADCIRC-CMIP6 models are negatively skewed in GSAT projections compared to the distribution of all 26 CMIP6 models (three are in the top 25%; Fig. S1 b), which may be leading to overly strong projections of compound changes at NYC. To explore potential selection bias, we compare the ADCRIC-CMIP6 projection that includes correlated changes (dark blue bars; Fig. 4 i-j) with a simple scaling relationship between ADCRIC-CMIP6 TC climatology change and GSAT change, that is applied to the projections of all 26 CMIP6 models (green bars on Fig. 4 i-j). At NYC the $\Delta\eta_{100}$ due to TC climatology change increases at a rate of 0.10 m (lowest 0.06 m; highest 0.15 m) and 0.02 m (lowest 0.008 m; highest 0.032 m) per degree GSAT change assuming frequency changes and no frequency change, respectively (Fig. S15 a,d). We apply these scaling relationships to the GSAT and relative SLR projections of all 26 CMIP6 models (Fig. S15 b-c,e-f). Specifically, we randomly sample one of the eight scaling factors (from the eight ADCIRC-CMIP6 models) and apply it to a randomly selected one of the 26 CMIP6 models based on its GSAT and add its SLR projection 100,000 times.

592

593

594

595

596

597

598

599

600

601

By comparing this scaling estimate with the ADCRIC-CMIP6 projection that includes correlated changes, we find that selection bias is leading to an over-estimated average projection of $\Delta\eta_{100}$ of 0.08 m (5%) and 0.03 m (3%) assuming frequency changes and no frequency change, respectively (Fig. 4 i-j). By comparing the average scaling estimate that includes correlation (dark green bars on Fig. 4 i-j) with the scaling estimate that doesn't include correlation (light green bars on Fig. 4 i-j), we also find that the average is under-estimated by 0.09 m (7%) and 0.06 m (6%) assuming frequency changes and no frequency change, respectively (Fig. 4 i-j). Additionally, the range is under-estimated by 0.17 m (11%) and 0.05 m (5%) when the positive correlation are neglected, assuming frequency change and no frequency change, respectively (Fig. 4 i-j).

602

603

604

605

606

607

608

609

610

611

We have found that by focusing on a subset of AOGCMs that do not reflect the full distribution of GSAT changes within the emission scenario, and by assuming independence between SLR and storm tide change, coastal flood hazard assessments may not accurately capture future coastal flood hazard. We recommend that future studies that focus on a specific emissions scenario: (1) construct SLR and TC projections inherent to each model to ensure that correlations are incorporated, (2) be mindful of the GSAT change and ECS of each CMIP6 model used, as selection bias may substantially alter flood hazard projections and (3) consider extremes as well as average projections, given that model variation is reduced when the correlation between SLR and TC projections are neglected.

4 Discussion

The results of this analysis indicate that flood hazard in the western North Atlantic and North West Pacific will increase substantially over the twenty first century due to relative SLR, compounded by TC climatology change. As shown in Marsooli et al. (2019), the effect of TC climatology change is likely to be larger than the effect of SLR for over 40% of coastal counties in the Gulf of Mexico. Additionally, the relative effect of TC climatology change increased continuously from New England, mid-Atlantic, southeast Atlantic, to the Gulf of Mexico. Effects on flooding of positive correlations between relative SLR and TC climatology found here, may therefore exhibit substantial spatial and temporal heterogeneity. For NYC, where SLR is considerably larger than projected TC surge change (see Section 3.3), neglecting correlated changes results in the average projected change to the historical 100-year flood level being under-estimated by 0.09 m (7%) and 0.06 m (6% of change) assuming frequency changes and no frequency changes, respectively. In some lower latitude regions that have higher projected TC climatology change compared to NYC (Marsooli et al., 2019), such as along the Gulf of Mexico and in parts of the western Pacific, neglecting positive correlations may lead to higher under-estimation of coastal flood hazard.

We also treat storm surge and SLR as linearly additive. This is problematic because interactions between SLR and surge and tides can potentially create a bias, up to the order of 15% in the future flood elevation, either high or low depending on exact geographic location (Resio & Irish, 2015). However, future SLR-TC interactions are expected to be small at NYC (Lin et al., 2012, 2010). Correlations between SLR and TC storm surge may also impact SLR-TC surge interactions; if changes to both SLR and TC storm surges are large then interactions between these components may also be stronger, further impacting future flood hazard. The spatial and temporal variability in correlations should be explored in future studies.

SLR and future TC activity will respond to radiative forcing, atmospheric feedbacks, the horizontal and vertical distribution of oceanic and atmospheric warming, and changes in climate oscillations, amongst others (Woodruff et al., 2013; Little et al., 2015). As the climate is a strongly coupled system, regional changes in climate forcing may be co-dependent (Lambert et al., 2021); and it is this co-dependence that imposes correlations between SLR and TC activity and associated coastal flooding. In this analysis, we do not attempt to rigorously explain correlations across the ensemble, as an individual model's response may be a combination of multiple drivers that have not been considered here. More efforts to clarify causal mechanisms and role of uncertainties are required to constrain the timescales and radiative forcing scenarios over which these correlations apply.

We also note that our results may be influenced by model selection bias, resulting from the fact that not all model output is available. To explore this, we compare GSAT projections of models used this study (26 models) to all available CMIP6 models that have surface temperature (tas) for the simulations and run used (34 in total; Fig. S1 c). The 26 CMIP6 models used here, span the full range of projected GSAT change, giving us some confidence that our results should be largely unaffected by the addition of other CMIP6 models. In addition, our results rely on a number of land ice SLR parameterizations that have considerable uncertainty. Ideally, our methodology would be applied to explicit model projections of all sea-level components, rather than parameterizations.

As the inter-model spread contributes a large fraction of the total projection uncertainty in SLR and TC activity, uncertainties may be reduced if outlier models can be shown to be unreliable (Little et al., 2015). In particular, our results indicate that the divergent behaviour of CMIP6 models in projections of future TC activity and relative SLR, is driven by models that project high ECS. Some high ECS models used in this study project more positive cloud feedback in response to increasing green-house gases, and

664 they also tend to have a stronger cooling effect from aerosol-cloud interactions (ACI) when
665 compared to low ECS models (Wang et al., 2021). These strong effects in the high ECS
666 models offset each other during much of the 20th century, when both anthropogenic aerosols
667 and emissions increased. However, these high ECS models poorly simulate the spatial
668 pattern of historical warming compared to low ECS models as aerosols are concentrated
669 in the Northern Hemisphere (Wang et al., 2021).

670 The compensating affects of strong ACI and cloud feedback in the high ECS mod-
671 els, which occurs over the historical period, does not occur into the future, as aerosols
672 are projected to decrease as greenhouse gases rise. CMIP6 models with more positive
673 cloud feedback, as a result, tend to have higher 21st century projected warming (Brunner
674 et al., 2020), ECS (Wang et al., 2021), and therefore, potentially higher SLR and future
675 TC activity. Indeed, we find that CMIP6 models that project the highest GMSLR and
676 globally averaged PI in this study also project the highest ECS and strongest cloud feed-
677 back (Fig. S16). If these high ECS and cloud-feedback models, which poorly simulate
678 the spatial pattern of historical warming, can be shown to be unrealistic, substantial un-
679 certainty reductions in projections (that are derived directly from CMIP6 models) of TC
680 activity and SLR, could result.

681 Finally, rain rates near the centres of TCs are also expected to increase with in-
682 creasing global temperatures (Knutson et al., 2015, 2020). The amount of TC related
683 rainfall that any given local area will experience is proportional to the rain rates and in-
684 versely proportional to the translation speeds of TCs (Kossin, 2018). Our projections
685 of slower moving storms along the US East Coast may therefore contribute to an increased
686 rate of rain in TCs in some regions (Gori et al., under review). In the northeast region
687 of the United States, especially in New England, coastal flooding induced by extra-tropical
688 cyclones (ETCs) are more frequent (but less destructive) than TC-induced flooding (Booth
689 et al., 2016). The effect of climate change on ETC storm surges is thought to be rela-
690 tively small on average along the US East Coast, although large uncertainties exist among
691 climate models (Lin et al., 2019). It is likely that correlations between relative SLR and
692 TC precipitation and ETC activity may well impact future flood hazard in some regions.

693 5 Conclusion

694 The results of this analysis indicate that relative SLR is correlated with aspects of
695 TC activity over much of the western North Atlantic and North West Pacific, suggest-
696 ing that progressive warming will compound future flood hazard in these regions. Increases
697 in PI, coupled with more favorable vertical wind shear also suggest a large scale envi-
698 ronment more conducive to TCs in these regions. Based on analyses of synthetic TCs
699 and hydrodynamic modeling, we find that large scale co-variability substantially impacts
700 local flood hazard at NYC, with future storm tides predicted to increase with warming
701 due to relative SLR coupled with progressively stronger and slower moving TCs along
702 the US East Coast, even if TC frequency remain unchanged.

703 We have found that by focusing on a subset of AOGCMs that do not reflect the
704 full distribution of GSAT changes within the emission scenario, and by assuming inde-
705 pendence between SLR and storm tide change, coastal flood hazard assessments may not
706 accurately capture future coastal flood hazard. By neglecting correlated changes, the av-
707 erage and range of projected change to the historical 100-year flood level is under-estimated
708 by 0.09 m (7%) and 0.17 m (11%), respectively. We recommend that future studies that
709 focus on a specific emissions scenario: (1) construct SLR and TC projections inherent
710 to each model to ensure that correlations are incorporated, (2) be mindful of the GSAT
711 change and ECS of each CMIP6 model used, as selection bias may substantially alter
712 flood hazard projections and (3) consider extremes as well as average projections, given
713 that model variation is reduced when the correlation between SLR and TC projections
714 are neglected.

715 Our paper is novel in that we explore global scale correlations between TC activ-
716 ity and relative SLR that includes contributions from land ice loss and associated GRD
717 fingerprints and from non-climatic changes. We also conduct climatology-hydrodynamic
718 modeling to quantify the impact of correlations on future flood hazard and explore cor-
719 relations between SLR and synthetic TCs. We show that aspects of TC activity change
720 are likely to co-vary with relative SLR, meaning that flood hazard assessments that ne-
721 glect the joint influence of these factors will misrepresent future flood hazard. We rec-
722 ommend that future studies on coastal flood hazards explore correlated changes between
723 future TCs, ETCs, precipitation and relative SLR.

724 **Acknowledgments**

725 We are grateful to D.J Rasmussen who provided helpful comments on the manuscript.
726 The authors thank T. Frederikse for providing output from the GRD model. JWL was
727 supported by the Princeton University Fellowship in Natural Sciences and Engineering.
728 REK was supported by NSF award ICER-1663807, NASA award 80NSSC20K1724, and
729 NASA JPL project 105393.509496.02.08.13.31. NL was supported by NSF award 1652448.
730 CMIP6 data is available from <https://esgf-node.llnl.gov/projects/cmip6/>. Out-
731 put from ADCIRC modeling is available from the authors upon reasonable request. Code
732 used in this analysis can be obtained at [https://github.com/JWLockwood/Lockwoodetal2021](https://github.com/JWLockwood/Lockwoodetal2021_Physdependence.git)
733 [_Physdependence.git](https://github.com/JWLockwood/Lockwoodetal2021_Physdependence.git).

734

References

735

Argus, D., Peltier, W., Drummond, R., & Moore, A. (2014, 05). The antarctica component of postglacial rebound model ice-6gc (vm5a) based on gps positioning, exposure age dating of ice thicknesses, and relative sea level histories.

736

737

738

Geophysical Journal International, 198, 537-563. doi: 10.1093/gji/ggu140

739

Aschwenden, A., Fahnestock, M. A., Truffer, M., Brinkerhoff, D. J., Hock, R., Khroulev, C., ... Khan, S. A. (2019). Contribution of the greenland ice sheet to sea level over the next millennium. *Science Advances*, 5(6), eaav9396.

740

741

742

doi: 10.1126/sciadv.aav9396

Bamber, J. L., Oppenheimer, M., Kopp, R. E., Aspinall, W. P., & Cooke, R. M. (2019). Ice sheet contributions to future sea-level rise from structured expert judgment. , 116(23). doi: 10.1073/pnas.1817205116

743

744

745

746

Bhatia, K., Vecchi, G., Murakami, H., Underwood, S., & Kossin, J. (2018). Projected response of tropical cyclone intensity and intensification in a global climate model. *Journal of Climate*, 31(20), 8281-8303. doi: 10.1175/JCLI-D-17-0898.1

747

748

749

750

Bilskie, M. V., Hagen, S. C., Alizad, K., Medeiros, S. C., Passeri, D. L., Needham, H. F., & Cox, A. (2016). Dynamic simulation and numerical analysis of hurricane storm surge under sea level rise with geomorphologic changes along the northern gulf of mexico. *Earth's Future*, 4(5), 177-193. Retrieved from <https://agupubs.onlinelibrary.wiley.com/doi/abs/10.1002/2015EF000347> doi: <https://doi.org/10.1002/2015EF000347>

751

752

753

754

755

756

Bilskie, M. V., Hagen, S. C., Medeiros, S. C., & Passeri, D. L. (2014). Dynamics of sea level rise and coastal flooding on a changing landscape. *Geophysical Research Letters*, 41(3), 927-934. Retrieved from <https://agupubs.onlinelibrary.wiley.com/doi/abs/10.1002/2013GL058759> doi: <https://doi.org/10.1002/2013GL058759>

757

758

759

760

761

Bister, M., & Emanuel, K. A. (1998). Dissipative heating and hurricane intensity. *Meteorology and Atmospheric Physics*, 65(3-4), 233-240. doi: 10.1007/BF01030791

762

763

764

765

766

767

Booth, J., Rieder, H., & Kushnir, Y. (2016, 09). Comparing hurricane and extra-tropical storm surge for the mid-atlantic and northeast coast of the united states for 1979-2013. *Environmental Research Letters*, 11, 094004. doi: 10.1088/1748-9326/11/9/094004

768

769

770

771

772

Brunner, L., Pendergrass, A. G., Lehner, F., Merrifield, A. L., Lorenz, R., & Knutti, R. (2020). Reduced global warming from cmip6 projections when weighting models by performance and independence. *Earth System Dynamics*, 11(4), 995-1012. Retrieved from <https://esd.copernicus.org/articles/11/995/2020/> doi: 10.5194/esd-11-995-2020

773

774

775

776

777

778

Buchanan, M., Kopp, R., Oppenheimer, M., & Tebaldi, C. (2016, August 1). Allowances for evolving coastal flood risk under uncertain local sea-level rise. *Climatic Change*, 137(3-4), 347-362. doi: 10.1007/s10584-016-1664-7

779

780

781

782

783

784

Camargo, S. J. (2013). Global and regional aspects of tropical cyclone activity in the CMIP5 models. *Journal of Climate*, 26(24), 9880-9902. doi: 10.1175/JCLI-D-12-00549.1

Camargo, S. J., & Wing, A. A. (2021). Increased tropical cyclone risk to coasts. *Science*, 371(6528), 458-459. doi: 10.1126/science.abg3651

Chan, J. C. (2005). The physics of tropical cyclone motion. *Annual Review of Fluid Mechanics*, 37(1), 99-128. doi: 10.1146/annurev.fluid.37.061903.175702

785

786

787

788

Chavas, D. R., Lin, N., & Emanuel, K. (2015). A model for the complete radial structure of the tropical cyclone wind field. part i: Comparison with observed structure. *Journal of the Atmospheric Sciences*, 72(9), 3647 - 3662. Retrieved from <https://journals.ametsoc.org/view/journals/atasc/72/9/jas-d-15-0014.1.xml> doi: 10.1175/JAS-D-15-0014.1

789

Chavas, D. R., Lin, N., & Emanuel, K. (2016). A model for the complete radial

- 789 structure of the tropical cyclone wind field . part ii : Wind field variability.
790 *Journal of the Atmospheric Sciences*, 72(9). doi: 10.1175/JAS-D-15-0185.1
- 791 Church, J., Clark, P., Cazenave, A., Gregory, J., Jevrejeva, S., Levermann, A., ...
792 Alakkat, U. (2013, 01). Climate change 2013: The physical science basis.
793 contribution of working group i to the fifth assessment report of the intergov-
794 ernmental panel on climate change. *Sea Level Change*, 1138-1191.
- 795 Coles, S. (2001). An introduction to statistical modeling of extreme values.
796 Cook, J. M., Tedstone, A. J., Williamson, C., McCutcheon, J., Hodson, A. J.,
797 Dayal, A., ... Tranter, M. (2020). Glacier algae accelerate melt rates on
798 the south-western greenland ice sheet. *The Cryosphere*, 14(1), 309–330. Re-
799 trieved from <https://tc.copernicus.org/articles/14/309/2020/> doi:
800 10.5194/tc-14-309-2020
- 801 De Dominicis, M., Wolf, J., Jevrejeva, S., Zheng, P., & Hu, Z. (2020). Fu-
802 ture Interactions Between Sea Level Rise, Tides, and Storm Surges in the
803 World's Largest Urban Area. *Geophysical Research Letters*, 47(4). doi:
804 10.1029/2020GL087002
- 805 Delhasse, A., Fettweis, X., Kittel, C., Amory, C., & Agosta, C. (2018). Brief com-
806 munication: Impact of the recent atmospheric circulation change in summer on
807 the future surface mass balance of the greenland ice sheet. *The Cryosphere*,
808 12(11), 3409–3418. Retrieved from [https://tc.copernicus.org/articles/](https://tc.copernicus.org/articles/12/3409/2018/)
809 [12/3409/2018/](https://tc.copernicus.org/articles/12/3409/2018/) doi: 10.5194/tc-12-3409-2018
- 810 Edwards, T. L., Nowicki, S., Marzeion, B., Hock, R., Goelzer, H., Seroussi, H., ...
811 Zwinger, T. (2021). Projected land ice contributions to 21st century sea level
812 rise. *Nature*, 593, 74–82. doi: 10.1038/s41586-021-03302-y
- 813 Emanuel. (2013). Downscaling CMIP5 climate models shows increased tropical
814 cyclone activity over the 21st century. *Proceedings of the National Academy of*
815 *Sciences of the United States of America*, 110(30), 12219–12224. doi: 10.1073/
816 pnas.1301293110
- 817 Emanuel. (2021). Response of global tropical cyclone activity to increasing co2: Re-
818 sults from downscaling cmip6 models. *Journal of Climate*, 34, 57-70.
- 819 Emanuel, & Nolan, D. S. (2004). Tropical cyclone activity and the global climate
820 system. *26th Conference on Hurricanes and Tropical Meteorology*(August),
821 240–241.
- 822 Emanuel, Sundararajan, R., & Williams, J. (2008, mar). Hurricanes and Global
823 Warming: Results from Downscaling IPCC AR4 Simulations. *Bulletin of the*
824 *American Meteorological Society*, 89(3), 347–368. Retrieved from [https://doi](https://doi.org/10.1175/BAMS-89-3-347)
825 [.org/10.1175/BAMS-89-3-347](https://doi.org/10.1175/BAMS-89-3-347) doi: 10.1175/BAMS-89-3-347
- 826 Eyring, V., Bony, S., Meehl, G. A., Senior, C. A., Stevens, B., Stouffer, R. J., &
827 Taylor, K. E. (2016). Overview of the coupled model intercomparison project
828 phase 6 (cmip6) experimental design and organization. *Geoscientific Model De-*
829 *velopment*, 9(5), 1937–1958. Retrieved from [https://gmd.copernicus.org/](https://gmd.copernicus.org/articles/9/1937/2016/)
830 [articles/9/1937/2016/](https://gmd.copernicus.org/articles/9/1937/2016/) doi: 10.5194/gmd-9-1937-2016
- 831 Farinotti, D., Huss, M., Fürst, J., Landmann, J., Machguth, H., Maussion,
832 F., & Pandit, A. (2019, 03). A consensus estimate for the ice thick-
833 ness distribution of all glaciers on earth. *Nature Geoscience*, 12. doi:
834 10.1038/s41561-019-0300-3
- 835 Fox-Kemper, B., Hewitt, H. T., Xiao, C., Aalgeirsdóttir, G., Drijfhout, S. S., Ed-
836 wards, T. L., ... Yu, Y. (2021). Ocean, cryosphere and sea level change.
837 in: Climate change 2021: The physical science basis. contribution of work-
838 ing group i to the sixth assessment report of the intergovernmental panel on
839 climate change. *Cambridge University Press.*
- 840 Frederikse, T., Buchanan, M. K., Lambert, E., Kopp, R. E., Oppenheimer, M., Ras-
841 mussen, D. J., & de Wal, R. S. (2020). Antarctic Ice Sheet and emission
842 scenario controls on 21st-century extreme sea-level changes. *Nature Com-*
843 *munications*, 11(1), 1–11. Retrieved from <http://dx.doi.org/10.1038/>

- 844 s41467-019-14049-6 doi: 10.1038/s41467-019-14049-6
- 845 Fürst, J. J., Goelzer, H., & Huybrechts, P. (2015). Ice-dynamic projections of the
846 greenland ice sheet in response to atmospheric and oceanic warming. *The*
847 *Cryosphere*, 9(3), 1039–1062. Retrieved from [https://tc.copernicus.org/
848 articles/9/1039/2015/](https://tc.copernicus.org/articles/9/1039/2015/) doi: 10.5194/tc-9-1039-2015
- 849 Garner, A. J., Mann, M. E., Emanuel, K. A., Kopp, R. E., Lin, N., Alley, R. B., ...
850 Pollard, D. (2017). Impact of climate change on new york city's coastal
851 flood hazard: Increasing flood heights from the preindustrial to 2300 ce.
852 *Proceedings of the National Academy of Sciences*, 114(45), 11861–11866.
853 Retrieved from <https://www.pnas.org/content/114/45/11861> doi:
854 10.1073/pnas.1703568114
- 855 Genthon, C., Krinner, G., & Castebunet, H. (2009). Antarctic precipitation and
856 climate-change predictions: horizontal resolution and margin vs plateau issues.
857 *Annals of Glaciology*, 50(50), 55–60. doi: 10.3189/172756409787769681
- 858 Gori, A., Lin, N., Xi, D., , & Emanuel, K. (under review). Tropical cyclone climatol-
859 ogy change greatly exacerbates us joint rainfall-surge hazard. *Nature Climate*
860 *Change*.
- 861 Gregory, Griffies, S. M., Hughes, C. W., Lowe, J. A., Church, J. A., Fukimori, I.,
862 ... Tamisiea, M. E. (2019). *Concepts and Terminology for Sea Level : Mean*
863 *, Variability and Change , Both Local and Global* (Vol. 0123456789). doi:
864 10.1007/s10712-019-09525-z
- 865 Gregory, & Huybrechts, P. (2006). Ice-sheet contributions to future sea-level change.
866 *Philosophical Transactions of the Royal Society A: Mathematical, Physical and*
867 *Engineering Sciences*, 364(1844), 1709-1732. doi: 10.1098/rsta.2006.1796
- 868 Griffies, S. M., Danabasoglu, G., Durack, P. J., Adcroft, A. J., Balaji, V., Böning,
869 C. W., ... Yeager, S. G. (2016). OMIP contribution to CMIP6: Experimental
870 and diagnostic protocol for the physical component of the Ocean Model Inter-
871 comparison Project. *Geoscientific Model Development*, 9(9), 3231–3296. doi:
872 10.5194/gmd-9-3231-2016
- 873 Griffies, S. M., & Greatbatch, R. J. (2012). Physical processes that impact the evo-
874 lution of global mean sea level in ocean climate models. *Ocean Modelling*, 51,
875 37–72. Retrieved from [http://dx.doi.org/10.1016/j.
876 doi: 10.1016/j.ocemod.2012.04.003](http://dx.doi.org/10.1016/j.ocemod.2012.04.003)
- 877 Griffies, S. M., Yin, J., Durack, P. J., Goddard, P., Bates, S. C., Behrens, E., ...
878 Zhang, X. (2014). An assessment of global and regional sea level for years
879 1993-2007 in a suite of interannual core-II simulations. *Ocean Modelling*, 78,
880 35–89. Retrieved from [http://dx.doi.org/10.1016/j.
881 doi: 10.1016/j.ocemod.2014.03.004](http://dx.doi.org/10.1016/j.ocemod.2014.03.004)
- 882 Hausfather, Z., & Peters, G. P. (2020). Heading in here running to two lines. *Na-*
883 *ture*.
- 884 Hermans, T. H. J., Gregory, J. M., Palmer, M. D., Ringer, M. A., Katsman, C. A.,
885 & Slangen, A. B. A. (2021). Projecting global mean sea-level change us-
886 ing cmip6 models. *Geophysical Research Letters*, 48(5), e2020GL092064.
887 Retrieved from [https://agupubs.onlinelibrary.wiley.com/doi/abs/
888 10.1029/2020GL092064](https://agupubs.onlinelibrary.wiley.com/doi/abs/10.1029/2020GL092064) (e2020GL092064 2020GL092064) doi: [https://
889 doi.org/10.1029/2020GL092064](https://doi.org/10.1029/2020GL092064)
- 890 Hock, R., Bliss, A., MARZEION, B., GIESEN, R. H., HIRABAYASHI, Y., HUSS,
891 M., ... SLANGEN, A. B. A. (2019). Glaciernip – a model intercompari-
892 son of global-scale glacier mass-balance models and projections. *Journal of*
893 *Glaciology*, 65(251), 453–467. doi: 10.1017/jog.2019.22
- 894 Hofer, S., Tedstone, A., Fettweis, X., & Bamber, J. (2019, 07). Cloud microphysics
895 and circulation anomalies control differences in future greenland melt. *Nature*
896 *Climate Change*, 9, 523. doi: 10.1038/s41558-019-0507-8
- 897 Hunter, J. (2011, 11). A simple technique for estimating an allowance for uncertain
898 sea-level rise. *Climatic Change*, 113. doi: 10.1007/s10584-011-0332-1

- 899 Idier, D., Bertin, X., Thompson, P., & Pickering, M. D. (2019). Interactions Between
900 Mean Sea Level, Tide, Surge, Waves and Flooding: Mechanisms and Contri-
901 butions to Sea Level Variations at the Coast. *Surveys in Geophysics*, 40(6),
902 1603–1630. Retrieved from <https://doi.org/10.1007/s10712-019-09549-5>
903 doi: 10.1007/s10712-019-09549-5
- 904 Joughin, I., Smith, B., & Medley, B. (2014, 05). Marine ice sheet collapse potentially
905 under way for the thwaites glacier basin, west antarctica. *Science (New York,
906 N.Y.)*, 344. doi: 10.1126/science.1249055
- 907 Kang, S. M., & Lu, J. (2012). Expansion of the hadley cell under global warm-
908 ing: Winter versus summer. *Journal of Climate*, 25(24), 8387 - 8393. Re-
909 trieved from [https://journals.ametsoc.org/view/journals/clim/25/24/
910 jcli-d-12-00323.1.xml](https://journals.ametsoc.org/view/journals/clim/25/24/jcli-d-12-00323.1.xml) doi: 10.1175/JCLI-D-12-00323.1
- 911 Khan, S., Björk, A., Bamber, J., Morlighem, M., Bevis, M., Kjær, K., ... Schenk,
912 T. (2020, 11). Centennial response of greenland's three largest outlet glaciers.
913 *Nature Communications*, 11. doi: 10.1038/s41467-020-19580-5
- 914 Kirezci, E., Young, I., Ranasinghe, R., Muis, S., Nicholls, R., Lincke, D., & Hinkel,
915 J. (2020, 07). Projections of global-scale extreme sea levels and resulting
916 episodic coastal flooding over the 21st century. *Scientific Reports*, 10, 11629.
917 doi: 10.1038/s41598-020-67736-6
- 918 Kittel, C., Amory, C., Agosta, C., Jourdain, N. C., Hofer, S., Delhasse, A., ... Fet-
919 tweis, X. (2021). Diverging future surface mass balance between the Antarctic
920 ice shelves and grounded ice sheet. , 1215–1236.
- 921 Knutson, Camargo, S. J., Chan, J. C. L., Emanuel, K., Ho, C.-H., Kossin, J., ...
922 Wu, L. (2020). Tropical Cyclones and Climate Change Assessment: Part II:
923 Projected Response to Anthropogenic Warming. *Bulletin of the American
924 Meteorological Society*, 101(3), E303–E322. Retrieved from [https://doi.org/
925 10.1175/BAMS-D-18-0194.1](https://doi.org/10.1175/BAMS-D-18-0194.1) doi: 10.1175/BAMS-D-18-0194.1
- 926 Knutson, Sirutis, J., Zhao, M., Tuleya, R., Bender, M., Vecchi, G., ... Chavas, D.
927 (2015). Global projections of intense tropical cyclone activity for the late
928 twenty-first century from dynamical downscaling of cimp5/rcp4.5 scenarios.
929 *Journal of Climate*, 28, 7203–7224.
- 930 Kopp, R. E., Deconto, R. M., Bader, D. A., Hay, C. C., Radley, M., Kulp, S., ...
931 Strauss, B. H. (2017). Earth ' s Future Evolving Understanding of Antarctic
932 Ice-Sheet Physics and Ambiguity in Probabilistic Sea-Level Projections Earth '
933 s Future.
- 934 Kopp, R. E., Hay, C. C., Little, C. M., & Mitrovica, J. X. (2015). Geographic Vari-
935 ability of Sea-Level Change. *Current Climate Change Reports*, 1(3), 192–204.
936 doi: 10.1007/s40641-015-0015-5
- 937 Kopp, R. E., Horton, R. M., Little, C. M., Mitrovica, J. X., Oppenheimer, M., Ras-
938 mussen, D. J., ... Tebaldi, C. (2014). Earth ' s Future Probabilistic 21st and
939 22nd century sea-level projections at a global network of tide-gauge sites Earth
940 ' s Future. , 383–407. doi: 10.1002/2014EF000239.Abstract
- 941 Kossin, J. P. (2018, June). A global slowdown of tropical-cyclone translation speed.
942 *Nature*, 558(7708), 104–107. Retrieved from [https://doi.org/10.1038/
943 s41586-018-0158-3](https://doi.org/10.1038/s41586-018-0158-3) doi: 10.1038/s41586-018-0158-3
- 944 Lambert, E., Le Bars, D., Goelzer, H., & van de Wal, R. S. (2021). Cor-
945 relations between sea-level components are driven by regional climate
946 change. *Earth's Future*, 9(2), e2020EF001825. Retrieved from [https://
947 agupubs.onlinelibrary.wiley.com/doi/abs/10.1029/2020EF001825
948 \(e2020EF001825 2020EF001825\)](https://agupubs.onlinelibrary.wiley.com/doi/abs/10.1029/2020EF001825) doi: <https://doi.org/10.1029/2020EF001825>
- 949 Levermann, A., Winkelmann, R., Albrecht, T., Goelzer, H., Golledge, N. R., Greve,
950 R., ... Van De Wal, R. S. (2020). Projecting Antarctica's contribution to
951 future sea level rise from basal ice shelf melt using linear response functions of
952 16 ice sheet models (LARMIP-2). *Earth System Dynamics*, 11(1), 35–76. doi:
953 10.5194/esd-11-35-2020

- 954 Li, Li, L., Ting, M., & Liu, Y. (2012, 09). Intensification of northern hemisphere
 955 near-surface subtropical highs in a warming climate. *Nature Geoscience*. doi:
 956 10.1038/ngeo1590
- 957 Li, Sun, C., & Jin, F.-F. (2013). Nao implicated as a predictor of northern hemi-
 958 sphere mean temperature multidecadal variability. *Geophysical Research Let-
 959 ters*, *40*(20), 5497-5502. doi: <https://doi.org/10.1002/2013GL057877>
- 960 Lin, N., Emanuel, K., Oppenheimer, M., & Vanmarcke, E. (2012). Physically based
 961 assessment of hurricane surge threat under climate change. *Nature Climate
 962 Change*, *2*, 462-467. doi: 10.1038/nclimate1389
- 963 Lin, N., Emanuel, K. A., Smith, J. A., & Vanmarcke, E. (2010). Risk assessment of
 964 hurricane storm surge for new york city. *Journal of Geophysical Research: At-
 965 mospheres*, *115*(D18). doi: <https://doi.org/10.1029/2009JD013630>
- 966 Lin, N., Kopp, R. E., Horton, B. P., & Donnelly, J. P. (2016). Hurricane sandy's
 967 flood frequency increasing from year 1800 to 2100. *Proceedings of the Na-
 968 tional Academy of Sciences*, *113*(43), 12071-12075. Retrieved from [https://](https://www.pnas.org/content/113/43/12071)
 969 www.pnas.org/content/113/43/12071 doi: 10.1073/pnas.1604386113
- 970 Lin, N., Marsooli, R., & Colle, B. (2019, 05). Storm surge return levels induced
 971 by mid-to-late-twenty-first-century extratropical cyclones in the northeastern
 972 united states. *Climatic Change*, *154*. doi: 10.1007/s10584-019-02431-8
- 973 Little, Horton, R. M., Kopp, R. E., Oppenheimer, M., Vecchi, G. A., & Villarini, G.
 974 (2015). Joint projections of US East Coast sea level and storm surge. *Nature
 975 Climatic Change*, *5*(12), 1114-1120. doi: 10.1038/nclimate2801
- 976 Liu, Y., Asher, T. G., & Irish, J. L. (2019). Physical drivers of changes in prob-
 977 abilistic surge hazard under sea level rise. *Earth's Future*, *7*(7), 819-832.
 978 Retrieved from [https://agupubs.onlinelibrary.wiley.com/doi/abs/](https://agupubs.onlinelibrary.wiley.com/doi/abs/10.1029/2019EF001216)
 979 [10.1029/2019EF001216](https://doi.org/10.1029/2019EF001216) doi: <https://doi.org/10.1029/2019EF001216>
- 980 Lu, J., Vecchi, G. A., & Reichler, T. (2007). Expansion of the hadley cell under
 981 global warming. *Geophysical Research Letters*, *34*(6).
- 982 Luettich, R., Jr, Westerink, J., & Scheffner, N. (1992, 11). Adcirc: An advanced
 983 three-dimensional circulation model for shelves, coasts, and estuaries. report
 984 1. theory and methodology of adcirc-2ddi and adcirc-3dl. *Dredging Research
 985 Program Tech. Rep. DRP-92-6*, 143.
- 986 Marsooli, R., & Lin, N. (2018). Numerical modeling of historical storm tides and
 987 waves and their interactions along the U.S. East and Gulf Coasts. *Jour-
 988 nal of Geophysical Research: Oceans*, *123*(5), 3844-3874. doi: 10.1029/
 989 2017JC013434
- 990 Marsooli, R., & Lin, N. (2020, 12). Impacts of climate change on hurricane flood
 991 hazards in jamaica bay, new york. *Climatic Change*, *163*, 1-19. doi: 10.1007/
 992 s10584-020-02932-x
- 993 Marsooli, R., Lin, N., Emanuel, K., & Feng, K. (2019). Climate change ex-
 994 acerbates hurricane flood hazards along US Atlantic and Gulf Coasts in
 995 spatially varying patterns. *Nature Communications*, *10*(1), 1-9. Re-
 996 trieved from <http://dx.doi.org/10.1038/s41467-019-11755-z> doi:
 997 10.1038/s41467-019-11755-z
- 998 Marzeion, B., Hock, R., Anderson, B., Bliss, A., Champollion, N., Fujita, K., ...
 999 Zekollari, H. (2020). Partitioning the uncertainty of ensemble projec-
 1000 tions of global glacier mass change. *Earth's Future*, *8*(7), e2019EF001470.
 1001 Retrieved from [https://agupubs.onlinelibrary.wiley.com/doi/abs/](https://agupubs.onlinelibrary.wiley.com/doi/abs/10.1029/2019EF001470)
 1002 [10.1029/2019EF001470](https://doi.org/10.1029/2019EF001470) (e2019EF001470 10.1029/2019EF001470) doi:
 1003 <https://doi.org/10.1029/2019EF001470>
- 1004 Merrill, R. T. (1988). Environmental influences on hurricane intensification.
 1005 *Journal of Atmospheric Sciences*, *45*(11), 1678 - 1687. Retrieved from
 1006 [https://journals.ametsoc.org/view/journals/atsc/45/11/1520-0469](https://journals.ametsoc.org/view/journals/atsc/45/11/1520-0469_1988_045_1678_eiohi_2_0_co_2.xml)
 1007 [_1988_045_1678_eiohi_2_0_co_2.xml](https://journals.ametsoc.org/view/journals/atsc/45/11/1520-0469_1988_045_1678_eiohi_2_0_co_2.xml) doi: 10.1175/1520-0469(1988)045<1678:
 1008 EIOHI>2.0.CO;2

- 1009 Oppenheimer, M., Glavovic, B., Hinkel, J., van de Wal, R., Magnan, A. K., Abd-
 1010 Elgawad, A., . . . Sebesvari, Z. (2019). Sea Level Rise and Implications for Low
 1011 Lying Islands, Coasts and Communities. *IPCC Special Report on the Ocean
 1012 and Cryosphere in a Changing Climate*, 355(6321), 126–129.
- 1013 Peltier, W. R., Argus, D. F., & Drummond, R. (2015). Space geodesy constrains
 1014 ice age terminal deglaciation: The global ice-6g_c (vm5a) model. *Journal of
 1015 Geophysical Research: Solid Earth*, 120(1), 450–487. Retrieved from [https://
 1016 agupubs.onlinelibrary.wiley.com/doi/abs/10.1002/2014JB011176](https://agupubs.onlinelibrary.wiley.com/doi/abs/10.1002/2014JB011176) doi:
 1017 <https://doi.org/10.1002/2014JB011176>
- 1018 Perrette, M., Landerer, F., Riva, R., Frieler, K., & Meinshausen, M. (2013). A scal-
 1019 ing approach to project regional sea level rise and its uncertainties. *Earth Sys-
 1020 tem Dynamics*, 4(1), 11–29. doi: 10.5194/esd-4-11-2013
- 1021 Rasmussen, D. J., Bittermann, K., Buchanan, M. K., Kulp, S., Strauss, B. H.,
 1022 Kopp, R. E., & Oppenheimer, M. (2018, mar). Extreme sea level impli-
 1023 cations of 1.5 °c, 2.0 °c, and 2.5 °c temperature stabilization targets in the
 1024 21st and 22nd centuries. *Environmental Research Letters*, 13(3), 034040.
 1025 Retrieved from <https://doi.org/10.1088/1748-9326/aaac87> doi:
 1026 10.1088/1748-9326/aaac87
- 1027 Reed, A. J., Mann, M. E., Emanuel, K. A., Lin, N., Horton, B. P., Kemp, A. C.,
 1028 & Donnelly, J. P. (2015). Increased threat of tropical cyclones and coastal
 1029 flooding to new york city during the anthropogenic era. *Proceedings of the Na-
 1030 tional Academy of Sciences*, 112(41), 12610–12615. Retrieved from [https://
 1031 www.pnas.org/content/112/41/12610](https://www.pnas.org/content/112/41/12610) doi: 10.1073/pnas.1513127112
- 1032 Resio, D. T., & Irish, J. L. (2015). Tropical Cyclone Storm Surge Risk. , 74–84. doi:
 1033 10.1007/s40641-015-0011-9
- 1034 Rignot, E., Mouginot, J., Morlighem, M., Seroussi, H., & Scheuchl, B. (2014).
 1035 Widespread, rapid grounding line retreat of pine island, thwaites, smith,
 1036 and kohler glaciers, west antarctica, from 1992 to 2011. *Geophysical Re-
 1037 search Letters*, 41(10), 3502–3509. Retrieved from [https://agupubs
 1038 .onlinelibrary.wiley.com/doi/abs/10.1002/2014GL060140](https://agupubs.onlinelibrary.wiley.com/doi/abs/10.1002/2014GL060140) doi:
 1039 <https://doi.org/10.1002/2014GL060140>
- 1040 Rios-Berrios, R., & Torn, R. D. (2017). Climatological analysis of tropical cyclone
 1041 intensity changes under moderate vertical wind shear. *Monthly Weather Re-
 1042 view*, 145(5), 1717 - 1738. Retrieved from [https://journals.ametsoc.org/
 1043 view/journals/mwre/145/5/mwr-d-16-0350.1.xml](https://journals.ametsoc.org/view/journals/mwre/145/5/mwr-d-16-0350.1.xml) doi: 10.1175/MWR-D-16
 1044 -0350.1
- 1045 Sobel, A. H., Camargo, S. J., Hall, T. M., Lee, C.-Y., Tippet, M. K., & Wing,
 1046 A. A. (2016). Human influence on tropical cyclone intensity. *Science*,
 1047 353(6296), 242–246. Retrieved from [https://science.sciencemag.org/
 1048 content/353/6296/242](https://science.sciencemag.org/content/353/6296/242) doi: 10.1126/science.aaf6574
- 1049 Tamisiea, M. E., & Mitrovica, J. X. (2011). The moving boundaries of sea level
 1050 change: Understanding the origins of geographic variability. *Oceanography*.
- 1051 Tang, B., & Camargo, S. J. (2014). Environmental control of tropical cy-
 1052 clones in cmip5: A ventilation perspective. *Journal of Advances in Mod-
 1053 eling Earth Systems*, 6(1), 115–128. Retrieved from [https://agupubs
 1054 .onlinelibrary.wiley.com/doi/abs/10.1002/2013MS000294](https://agupubs.onlinelibrary.wiley.com/doi/abs/10.1002/2013MS000294) doi:
 1055 <https://doi.org/10.1002/2013MS000294>
- 1056 Tebaldi, C., Strauss, B. H., & Zervas, C. E. (2012, mar). Modelling sea level rise im-
 1057 pacts on storm surges along US coasts. *Environmental Research Letters*, 7(1),
 1058 014032. Retrieved from <https://doi.org/10.1088/1748-9326/7/1/014032>
 1059 doi: 10.1088/1748-9326/7/1/014032
- 1060 Ting, M., Kossin, J., Camargo, S., & Li, C. (2019, 05). Past and future hurricane in-
 1061 tensity change along the u.s. east coast. *Scientific Reports*, 9. doi: 10.1038/
 1062 s41598-019-44252-w
- 1063 Trenberth, K., Fasullo, J., & Shepherd, T. (2015, 07). Attribution of climate ex-

- 1064 tremente events. *Nature Climate Change*, 5, 725-730. doi: 10.1038/nclimate2657
- 1065 Vecchi, G. A., Delworth, T. L., Murakami, H., Underwood, S. D., Wittenberg,
1066 A. T., Zeng, F., ... Yang, X. (2019). *Tropical cyclone sensitivities to CO2*
1067 *doubling: roles of atmospheric resolution, synoptic variability and back-*
1068 *ground climate changes* (Vol. 53) (No. 9-10). Springer Berlin Heidelberg.
1069 Retrieved from <https://doi.org/10.1007/s00382-019-04913-y> doi:
1070 10.1007/s00382-019-04913-y
- 1071 Vecchi, G. A., & Soden, B. J. (2007a). Effect of remote sea surface temperature
1072 change on tropical cyclone potential intensity. *Nature*, 450, 1066-1070.
- 1073 Vecchi, G. A., & Soden, B. J. (2007b). Global warming and the weakening of
1074 the tropical circulation. *Journal of Climate*, 20(17), 4316 - 4340. Re-
1075 trieved from [https://journals.ametsoc.org/view/journals/clim/20/](https://journals.ametsoc.org/view/journals/clim/20/17/jcli4258.1.xml)
1076 [17/jcli4258.1.xml](https://journals.ametsoc.org/view/journals/clim/20/17/jcli4258.1.xml) doi: 10.1175/JCLI4258.1
- 1077 Vecchi, G. A., & Soden, B. J. (2007c). Increased tropical Atlantic wind shear in
1078 model projections of global warming. *Geophysical Research Letters*, 34(8), 1-5.
1079 doi: 10.1029/2006GL028905
- 1080 Vega-Westhoff, B., Sriver, R. L., Hartin, C., Wong, T. E., & Keller, K. (2020). The
1081 role of climate sensitivity in upper-tail sea level rise projections. *Geophys-*
1082 *ical Research Letters*, 47(6), e2019GL085792. Retrieved from [https://](https://agupubs.onlinelibrary.wiley.com/doi/abs/10.1029/2019GL085792)
1083 agupubs.onlinelibrary.wiley.com/doi/abs/10.1029/2019GL085792
1084 (e2019GL085792 2019GL085792) doi: <https://doi.org/10.1029/2019GL085792>
- 1085 Villarini, G., & Vecchi, G. A. (2013). Projected increases in North Atlantic tropical
1086 cyclone intensity from CMIP5 models. *Journal of Climate*, 26(10), 3231-3240.
1087 doi: 10.1175/JCLI-D-12-00441.1
- 1088 Vousdoukas, M., Mentaschi, L., Voukouvalas, E., Verlaan, M., Jevrejeva, S., Jackson,
1089 L., & Feyen, L. (2018, 06). Global probabilistic projections of extreme sea
1090 levels show intensification of coastal flood hazard. *Nature Communications*, 9.
1091 doi: 10.1038/s41467-018-04692-w
- 1092 Wahl, T., Jain, S., Bender, J., Meyers, S. D., & Luther, M. E. (2015). Increasing
1093 risk of compound flooding from storm surge and rainfall for major US cities.
1094 *Nature Climate Change*, 5(12), 1093-1097. doi: 10.1038/nclimate2736
- 1095 Wang, Soden, B. J., Yang, W., & Vecchi, G. A. (2021). Compensation between
1096 cloud feedback and aerosol-cloud interaction in cmip6 models. *Geophys-*
1097 *ical Research Letters*, 48(4), e2020GL091024. Retrieved from [https://](https://agupubs.onlinelibrary.wiley.com/doi/abs/10.1029/2020GL091024)
1098 agupubs.onlinelibrary.wiley.com/doi/abs/10.1029/2020GL091024
1099 (e2020GL091024 2020GL091024) doi: <https://doi.org/10.1029/2020GL091024>
- 1100 Wang, & Toumi, R. (2021). Recent migration of tropical cyclones toward coasts.
1101 *Science*, 371(6528), 514-517. doi: 10.1126/science.abb9038
- 1102 Westerink, J., Luettich, R., Jr, Blain, C., & Scheffner, N. (1994, 01). Adcirc: An
1103 advanced three-dimensional circulation model for shelves, coasts, and estuaries.
1104 report 2. user's manual for adcirc-2ddi. , 168.
- 1105 Woodruff, J. D., Irish, J. L., & Camargo, S. J. (2013). Coastal flooding by
1106 tropical cyclones and sea-level rise. *Nature*, 504(7478), 44-52. doi:
1107 10.1038/nature12855
- 1108 Yamada, Y., Oouchi, K., Satoh, M., Tomita, H., & Yanase, W. (2010). Projection of
1109 changes in tropical cyclone activity and cloud height due to greenhouse warm-
1110 ing: Global cloud-system-resolving approach. *Geophysical Research Letters*,
1111 37(7), 1-5. doi: 10.1029/2010GL042518
- 1112 Yin, J., Griffies, S. M., Winton, M., Zhao, M., & Zanna, L. (2020). Response of
1113 Storm-Related Extreme Sea Level along the U.S. Atlantic Coast to Com-
1114 bined Weather and Climate Forcing. *Journal of Climate*, 33(9), 3745-
1115 3769. Retrieved from <https://doi.org/10.1175/JCLI-D-19-0551.1> doi:
1116 10.1175/JCLI-D-19-0551.1
- 1117 Zelinka, M. D., Myers, T. A., McCoy, D. T., Po-Chedley, S., Caldwell, P. M.,
1118 Ceppi, P., ... Taylor, K. E. (2020). Causes of higher climate sensitivity

- 1119 in cmip6 models. *Geophysical Research Letters*, 47(1), e2019GL085782.
1120 Retrieved from [https://agupubs.onlinelibrary.wiley.com/doi/abs/](https://agupubs.onlinelibrary.wiley.com/doi/abs/10.1029/2019GL085782)
1121 10.1029/2019GL085782 (e2019GL085782 10.1029/2019GL085782) doi:
1122 <https://doi.org/10.1029/2019GL085782>
- 1123 Zscheischler, J., & Seneviratne, S. I. (2017). Dependence of drivers affects risks as-
1124 sociated with compound events. *Science Advances*, 3(6), 1–11. doi: 10.1126/
1125 sciadv.1700263
- 1126 Zscheischler, J., Westra, S., van den Hurk, B. J. J. M., Seneviratne, S. I., Ward,
1127 P. J., Pitman, A., ... Zhang, X. (2018). Future climate risk from compound
1128 events. *Nature Climate Change*, 8(6), 469–477. Retrieved from [https://](https://doi.org/10.1038/s41558-018-0156-3)
1129 doi.org/10.1038/s41558-018-0156-3 doi: 10.1038/s41558-018-0156-3

1130 **6 Tables**

Model	ECS (°C)	GSAT (°C)	Annual frequency	SLR (m)	RMW (%)	PI (%)	TS (%)
GFDL-ESM4	2.6	3.6	0.23	0.68	-11	7.6	-5.9
MIROC6	2.6	4.0	0.53	0.84	-10	8.8	-8.1
MPI-ESM1-2-HR	3.0	3.6	0.26	0.86	-9.3	8.8	-11
MRI-ESM2-0	3.2	4.3	0.13	0.95	-19	22	-13
EC-Earth3	4.3	5.3	2.0	0.97	-22	38	-24
CNRM-CM6-1	4.6	5.6	0.60	1.0	-14	36	-15
IPSL-CM6A-LR	4.6	6.0	1.2	1.0	-18	38	-18
CanESM5	5.6	7.0	0.34	1.1	-15	25	-29

Table 1. Modeled global ECS (°C) and projected changes in relative SLR (m) and TC characteristics at NYC for the CMIP6 subset modeled with ADCIRC. RMW, PI and TS denote the radius of maximum wind speed, maximum wind speed and translation speed, respectively. Estimates of ECS are from Zelinka et al. (2020) and Wang et al. (2021). Change is calculated as the difference between years 1994-2014 of the historical simulation and years 2080-2100 of the high emissions SSP5-8.5.

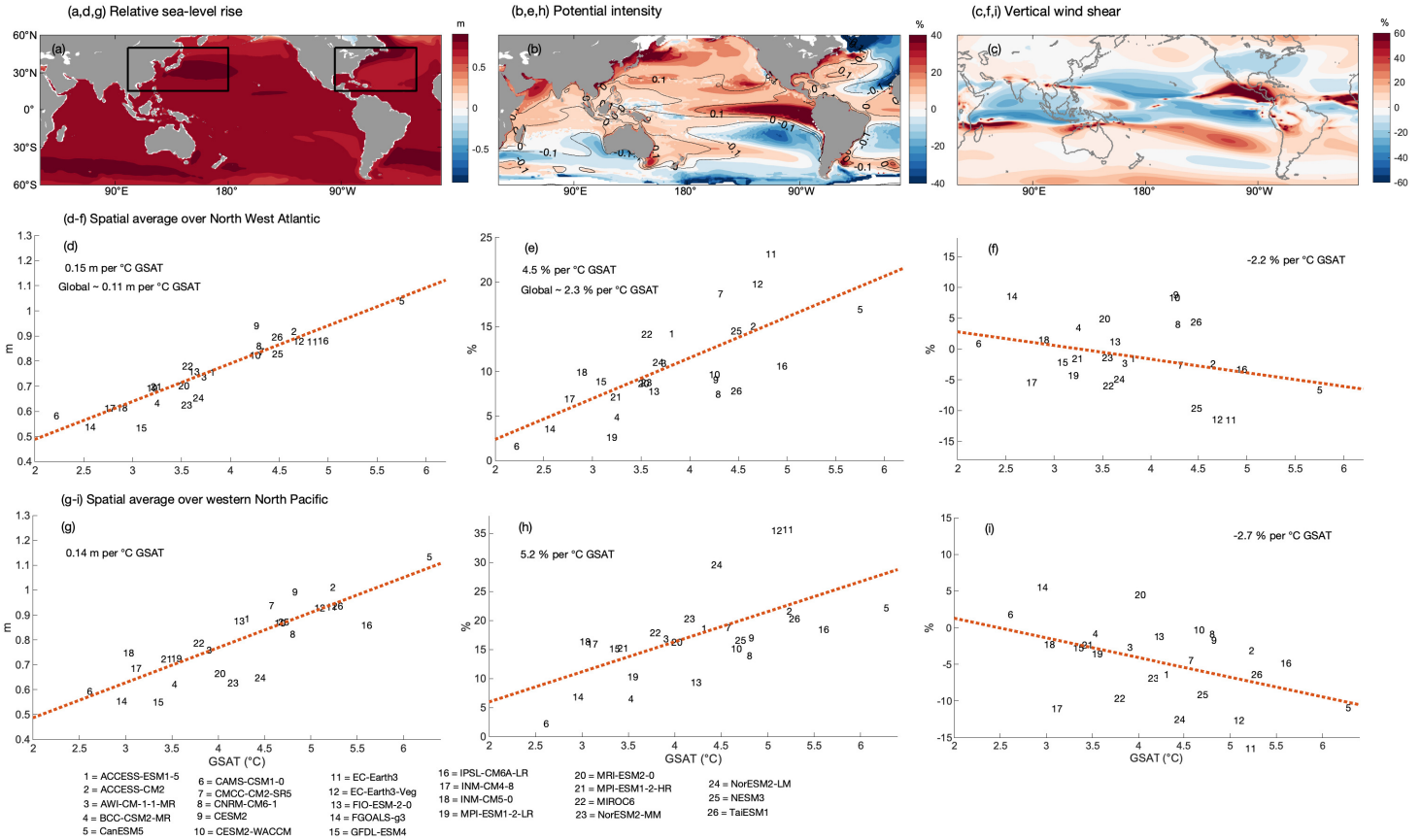


Figure 1. Panels (a–c) show the ensemble mean response of relative sea-level rise (a), potential intensity (b) and vertical wind shear (c). Potential intensity and vertical wind shear are displayed as percentage increases from years 1994–2014 of the historical simulation. Anomalies in potential intensity and vertical wind shear in the Northern Hemisphere are computed over June through November, while anomalies in the Southern Hemisphere are computed over December through May. Contours in (b) show the normalized departure of the local SST change from the tropical-mean (averaged over 35°S – 35°N) SST change. Scatter plots show the spatial averages over the western North Atlantic (d–f) and North West Pacific (e–i): each dot represents a single model. The solid black boxes in (a) show the North West Pacific and western North Atlantic regions.

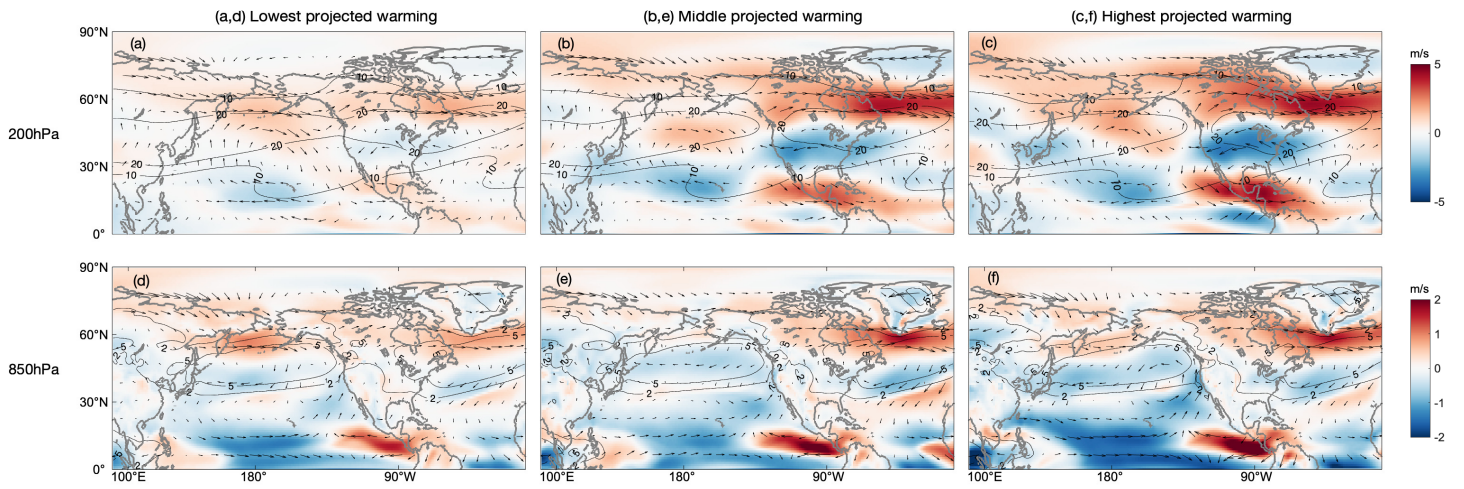


Figure 2. Composites of June-November mean 200hPa (top) and 850 hPa (bottom) horizontal wind vector differences between the average for the SSP5-8.5 (2080-2100) and the historical period (1994-2014). Background colors show speed changes and contours show historical zonal winds. Composites are based on projected GSAT warming. (a,d) Lowest project warming being the average over the models with the lowest third of projected GSAT change; (c,f) highest projected warming models being the average over the top third of project GSAT changes. Anomalies are computed over June through November.

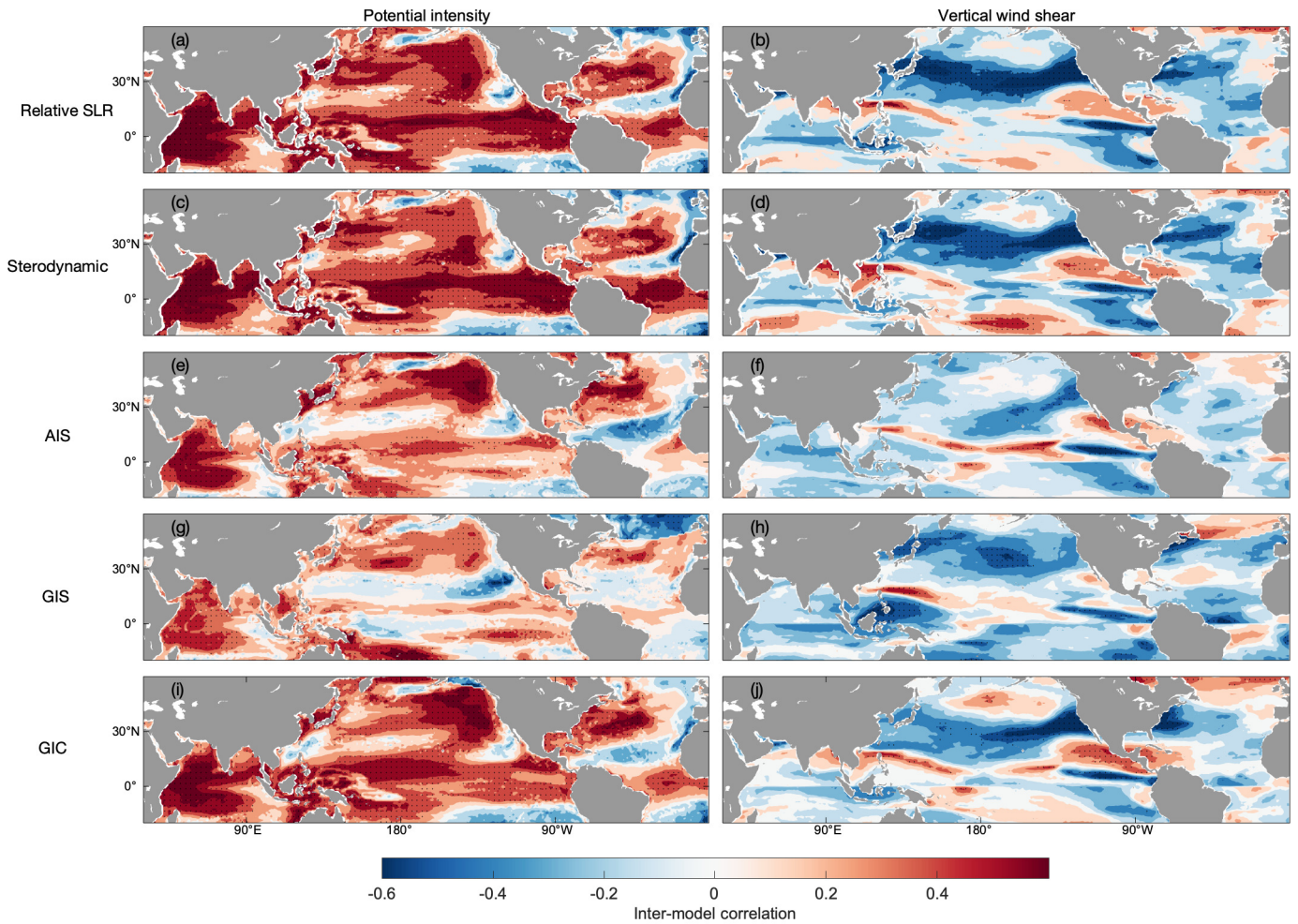


Figure 3. Inter-model correlations between sea-level rise (rows) and potential intensity (left column) and vertical wind shear (right column) for all 26 CMIP6 models. Rows show each component of SLR: relative sea-level rise (a-b), sterodynamic (c-d), Antarctic (e-f), Greenland (g-h) and Glaciers and Ice caps (i-j). Stipples denote correlations significant to 95%.

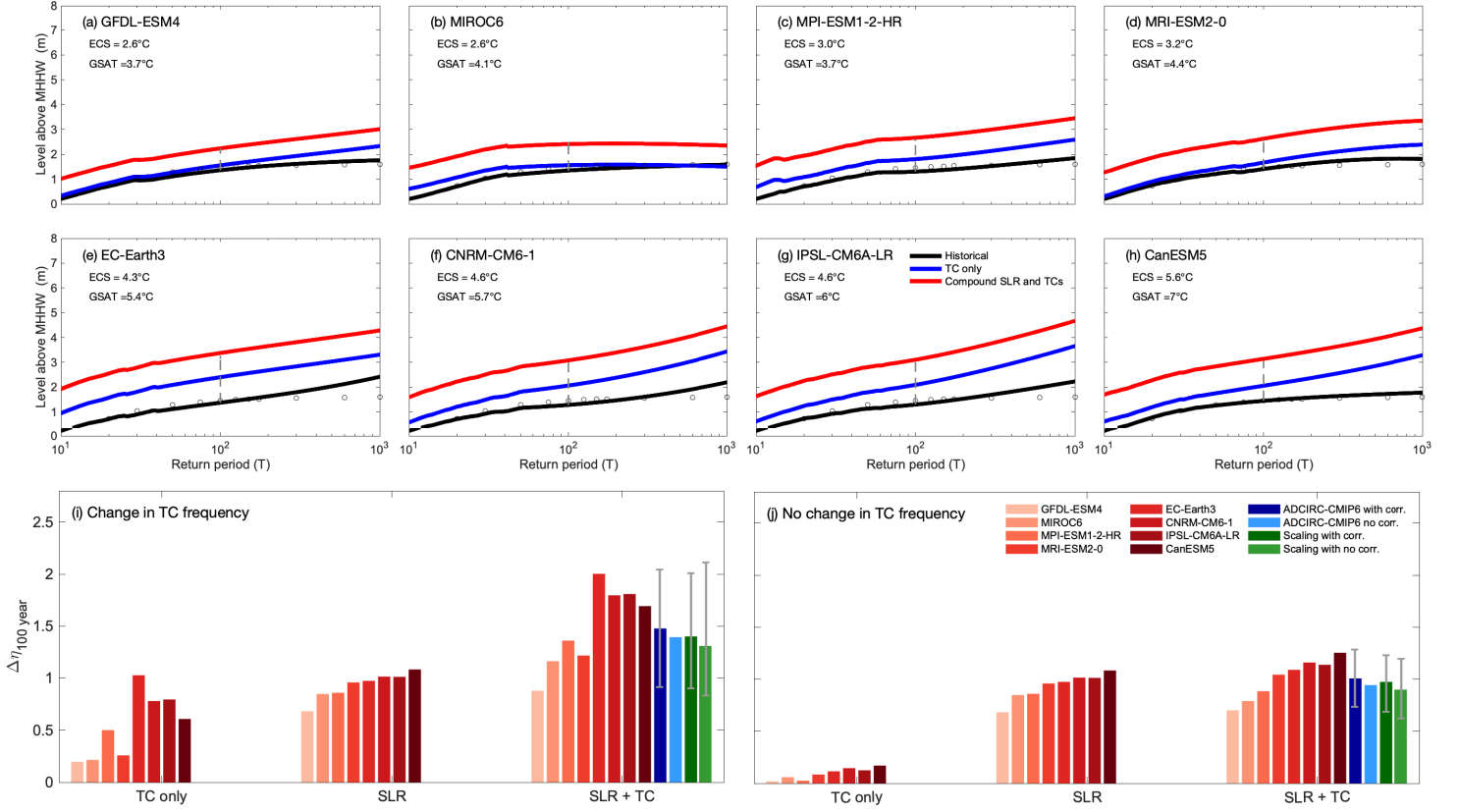


Figure 4. Estimated storm tide return levels for the historical period of 1994–2014 (black) and future period of 2080–2100 (blue: only effects of TC changes, red: compound effects of SLR and TCs) at New York City (a–h). Models are ordered by ascending ECS (Table. 1). Bar charts show the contributions to the change in the 100 year historical storm level, assuming (i) change and (j) no change in TC frequency at NYC. Fig. S10 shows the return period figures assuming no change in frequency of TCs. Storm tide levels are relative to mean higher high water (MHHW, obtained from <https://vdatum.noaa.gov>). The dark blue bars on (i–j) show the mean of the ADCIRC-CMIP6 models that includes correlated changes, whilst the light blue bars show the ADCIRC-CMIP6 projection constructed through convolution (i.e. neglecting correlations). The green bars on (i–j) show the compound changes derived from the scaling method based on the GSAT and SLR projections of all 26 CMIP6 models as described in Section 3.3.3, with the dark green denoting correlated changes and light green neglecting correlated changes. Black dots on (a–h) are empirical estimates. Vertical grey bars (i–j) denote the model ranges.

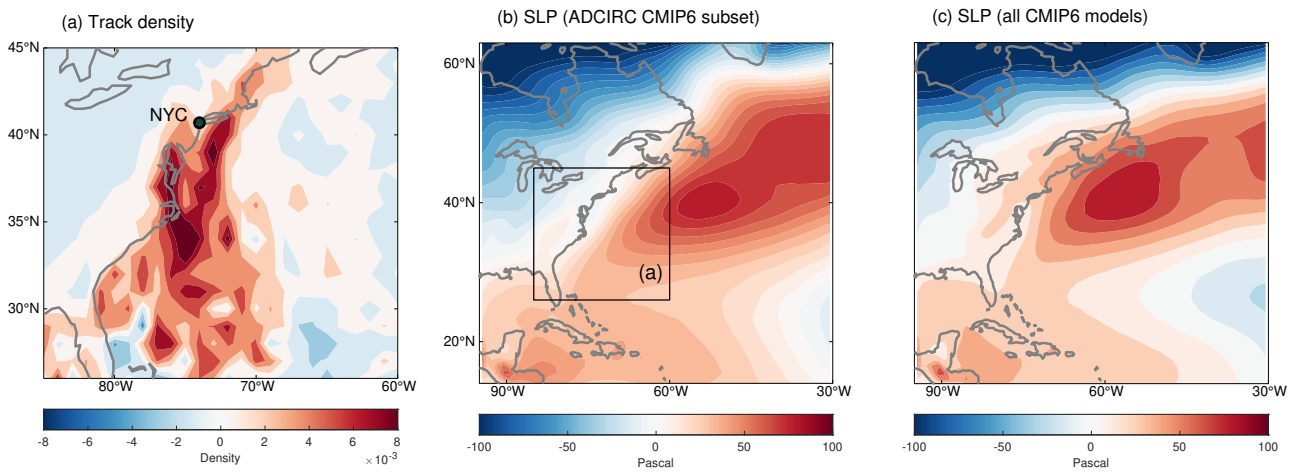


Figure 5. Multimodel mean difference between future and modern synthetic TC track densities assuming no change in TC frequency at NYC (a). Track densities are determined by the sum total of tracks crossing through each grid box over 20-year periods from 2080–2100 and 1994–2014, divided by the area of that grid box and the number of years. (b-c) Mean sea-level pressure (SLP) differences (pascals) averaged over June - November for the eight CMIP6 modeled with ADCIRC (b) and for all 26 CMIP6 used in this study (c).

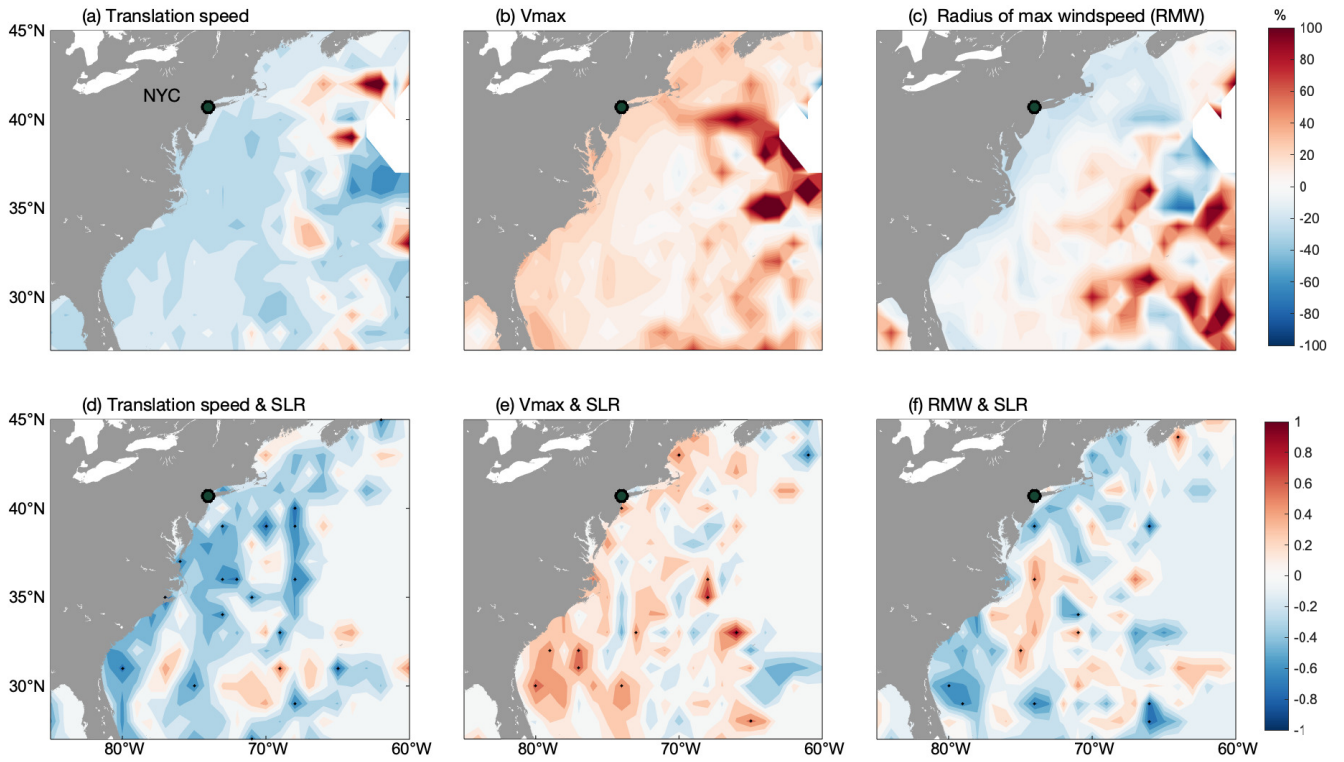


Figure 6. (a-c) Multimodel mean projected changes in TC intensity, radius of maximum wind and speed translation speed shown as percentage increases from years 1994-2014 of the historical simulation. (d-f) Inter-model correlations between projected changes in TC characteristics and relative SLR.